Thermal Behavior of Composite Superconductors and an Advanced Winding Method for Large Superconducting Helical Coils

Tomoyuki Senba

DOCTOR OF PHILOSOPHY

Department of Fusion Science
School of Mathematical and Physical Science
The Graduate University for Advanced Studies

1995 (School Year)

Thermal Behavior of Composite Superconductors and an Advanced Winding Method for Large Superconducting Helical Coils

Tomoyuki Senba

Dissertation

submitted in partial fulfillment of the requirements

for the degree of

DOCTOR OF PHILOSOPHY

Department of Fusion Science
School of Mathematical and Physical Science
The Graduate University for Advanced Studies
1995 (School Year)

Abstract

A crucial issue concerning the reliability of large superconducting magnets for next generation fusion devices is the stability of their superconductivity. There is a certain current, called the *recovery current*, below which superconductivity is restored if a conductor has reverted to a normal state. There is a minimum disturbance energy, called the *minimum quench energy (MQE)*, which causes a quench, a complete reversion to the normal state, if the magnet is operating at a current above the recovery current. If the magnet is operating at a current below the recovery current, it will not quench as long as its conductors are sufficiently cooled.

This thesis proposes the improvement of MQE evaluation methods for superconductors and the employment of an advanced winding method for superconducting helical coils. The object of our studies was the Large Helical Device (LHD) of the National Institute for Fusion Science (NIFS); however, improving MQE evaluation is extremely important to any large-scale superconducting magnet, and improving coil winding raises the MQE of any superconducting coil system.

When investigating the thermal behavior of composite superconductors, we obtained accurate MQE values by considering the following:

1. Experimental MQE values usually contain errors caused mainly by the fact that the response times of heating devices are longer than the thermal diffusion time constants of conductor materials. These errors can be eliminated by two-dimensional thermal analysis. The computed MQE value was smaller than the measured MQE value by one order.
2. The stability margin of a conductor varies with the direction of the heat flux when the conductor is marked by anisotropy, which in the one used in LHD helical coils derives from its geometry. The computed MQE value was smaller because the anisotropy of the conductor had been taken into account.

3. When the disturbances in a magnet are distributed, an accurate MQE value can still be obtained by employing an experimental formula. The MQE value per heated spot at distributed disturbances approaches half of the value at point disturbance, and total energy increases with the number of heated spots.

When developing an advanced winding method for superconducting helical coils, we aimed at preventing degradation of the coils, in particular, at reducing the magnitude and probability of mechanical disturbances in the coils:

1. Experimental helical coil windings demonstrated the necessity of adjusting the shape of the conductors continuously and to create tension in the coil deliberately.
2. A real-scale winding trial was carried out. It demonstrated the effectiveness of our newly developed method, which utilizes the three-dimensional shape of helical coils and makes it possible to create tension after the usual winding process, leading to superior coil winding accuracy.

Our method can be applied to the manufacturing process of any helical coil, but it is particularly valuable for superconducting helical coils with cooling channels.

When evaluating the cryogenic stability of the LHD helical coils, we found that degradation in coil performance will in all likelihood be limited to an acceptable degree, contrary to the previously constructed experimental coils for LHD. With substantially improved winding accuracy, the windings are expected to be mechanically rigid enough to withstand the electromagnetic force acting on them when the coils are energized. With a larger proportion of wet to total conductor surface than in the short samples, cooling is expected to be improved enough to raise the recovery current even above the rated current of the coil.

When evaluating the coil performance on an operating current just above the rated current, we found that the permissible disturbance energy will be several tens of mJ. This means that the permissible wire movement would be between several μm and several tens of μm. Although the winding accuracy we achieved with our new technique still leaves space for greater wire movement than that, the electromagnetic force acting on the conductors during energization up to the rated current will effectively reduce the gaps between them and thus further enhance the mechanical rigidity of the windings. This means that the actual wire movement may well be restricted to an extent corresponding with the permissible disturbance energy. Cooling with superfluid helium will greatly help to raise the recovery current of the coils above the rated current.

Having made these contribution to the design, construction, and operation of superconducting magnets, we believe that important next steps will be to learn how liquid and gaseous helium behave in finite cooling channels and to clarify how these channels affect the cryogenic stability of superconducting magnets.

Acknowledgments

I wish to thank my supervisor, Professor Osamu Motojima, for his valuable advice and guidance in my work. I also wish to thank my advisor, Associate Professor Satarou Yamaguchi, for his expert advice and continuous support.

I acknowledge the advice and encouragement I received from Professor Junya Yamamoto.

I am grateful to Director General Atsuo Iiyoshi for the opportunity to study at the National Institute for Fusion Science.

Many thanks to the staff of the National Institute for Fusion Science for their support and to my fellow students from the University for Advanced Studies and the Nagoya University for their help. Many thanks also to my colleagues at Hitachi for their help and to my company for their financial support.

I thank my parents and my family, to whom I dedicate this work.

Table of Contents

1. Introduction

This thesis presents analytical and experimental work on evaluating and improving the stability of superconducting magnets for large fusion devices. The two key issues were the assessment of the minimum quench energy (MQE) in a superconductor and the development of an advanced winding method for helical coils. The goal was to improve the design criteria for superconducting magnets in large fusion devices.

1-1. Helical Coils in Fusion Devices

Thermonuclear fusion has been studied for nearly half a century as the next generation means of energy production. The most promising route towards the commercial production of power now seems to be magnetic confinement of a hot deuterium-tritium plasma. There are several types of magnetic confinement systems, but toroidal systems, which utilize toroidally nested magnetic surfaces to confine the hot plasma, play the leading role. One group are tokamaks. They apply the principal of transformers to generate toroidal plasma current and are thus pulse-operated. Another group are helical devices like heliotrons (or torsatrons) and stellarators, which are the main alternatives to tokamaks [1]. They employ solely the currents in their external coils to generate magnetic configurations for plasma confinement. Unlike tokamaks, they allow net current-free plasma operation and are thus well suited to the continuous performance of a reactor. Heliotrons have been developed in Japan for more than thirty years as their magnetic configuration is superior to other magnetic configurations on a built-in divertor without divertor coils. After experiences with heliotrons like the Heliotron-E and the Compact Helical System (CHS), the Japanese Ministry of Education approved the Large Helical Device (LHD) as a national project in 1989 [2]. It is now under construction in Toki, the new location of the National Institute for Fusion Science (NIFS) [3].

The shape and position of their magnetic surfaces are decided by the currents of the helical coils and coil winding accuracy affects the plasma confinement properties of heliotrons significantly [4]. The recent trend requiring magnets in fusion devices to be superconductive makes even stronger demands on the accuracy and continuity of helical coils. However, their complex shape and the needs to improve superconducting performance and to reduce heat loads generated by ohmic heating at cooling joints poses engineering difficulties for the art of continuous helical winding and for the manufacture of helical coils [5][6]. This is one of the key issues of this study.

1-2. Superconducting Magnets in Fusion Devices

As fusion devices have grown in size requiring a longer energy confinement time, their energy consumption through ohmic heating in their conventional magnets has also grown larger; this has reduced their efficiency as power generation devices. Hence next generation fusion devices require superconducting magnets for their intrinsic no-energy dissipation. The development of experimental fusion devices with superconducting magnets has been a strong motivation to develop stable and high-current composite superconductors for electrical power use. The leading superconducting fusion devices are the TRIAM-1M at Kyushu University [7] and the Tore Supra at the Centre d'Etudes de Cadarache [8]. Both of them are tokamaks, and only their toroidal field magnets are superconductive. The TRIAM-1M has conductors with Nb_3Sn, a practicable superconducting material with excellent characteristics in high magnetic fields, and a cooling system with saturated liquid helium, the most popular cryogen. The Tore Supra has conductors with NbTi, the most popular practicable superconducting material, and a cooling system with superfluid helium, a cryogen with excellent characteristics in advanced, more efficient cooling technologies. The two fusion devices have a magnetic stored energy of between several tens of MJ and several hundred MJ. Efforts to develop larger superconducting magnets for fusion devices are being made [9], however these two are the only ones in operation to date. Superconducting toroidal field magnets, operated on dc currents, were developed earlier than pulse-operated poloidal field magnets, because the latter suffer considerable as losses, which still poses one of the difficulties for the development of superconducting magnets.

In order to take greater advantages of the steady-state operation of helical devices, efforts to develop superconducting helical devices are being made. There are two projects [10]: our LHD is under construction and the construction of the Wendelstein VII-X has been approved [11]. The LHD is the first experimental fusion device and the first helical device in which all coils, both the helical and the poloidal field coils, are superconductive [12]. At 1.6 GJ, it also has the largest magnetic stored energy of all superconducting magnets [13]. Design and construction of the LHD thus present great challenges illustrated by the complex shape of its helical coils and its large poloidal field coils. Their conductors must satisfy rated currents, and their coils must satisfy standards concerning geometrical accuracy that guarantees their magnetic field profile, concerning mechanical rigidity that enables them to withstand strong electromagnetic force, and cryogenic qualities that allow sufficient cooling for their superconducting stability.

Reliability is the most important requirement which the majority of large superconducting magnets must meet, and the LHD is no exception. One of the crucial issues concerning the reliability of superconducting magnets is their superconducting stability. A disturbance in a superconducting magnet may cause a quench, i.e. the complete reversion from the superconducting to the normal state. It occurs when a heat input raises the temperature of a superconductor enough to create a local normal zone, which then propagates throughout the entire magnet. The disturbance energy release may be due to the magnetic instability of the superconducting material, or cracks in the epoxy impregnation of the windings, or frictional heating caused by wire movements in the magnet, or ohmic heating caused by ac losses in a conductor. In large, pool-cooled, superconducting magnets for fusion devices, like the LHD helical coils, frictional heating from wire movements is considered to be the dominant origin of disturbance energy release. A quench encompasses the abrupt release of the stored magnetic energy, which may damage the magnet.

Superconducting magnets are designed to avoid quenches. Experimental and analytical methods should be employed to ensure the superconducting stability of their conductors. This is the other key issue of this study.

1-3. Reasons for this Study

Large superconducting magnets are often designed to operate below a current at which the superconducting state is consistently restored; this current is called the recovery current. The LHD helical coils, too, are designed on this criterion. If a normal zone appears in a conductor which is intended to operate below the recovery current, the conductor returns to the superconducting state and it does not come to a quench. However, this is not assured in the following cases, in which the operation current of the magnet exceeds its recovery current.

(1) The recovery current of the magnet is lower than the estimated recovery current of its conductors.

(2) The operation current of the magnet has been increased over its recovery current for an improved magnetic field profile.

The first case is an inherent problem of conductor evaluation. The second case is a challenging scenario for magnet operation only possible after the rated current has been attained.

There are a number of factors relevant to both cases: (a) The winding process may have degraded the performance of the conductors through an increase in resistivity of their stabilizers, damage to their superconducting strands, or a change in the surfaces of the conductors. (b) The recovery current of the magnet may have been lowered below the recovery current of its conductors, e.g. excessive conductor movement, caused by electromagnetic force and made possible by poor winding accuracy, could have generated extreme heat [14][15]. (c) The recovery current may initially have been overestimated because the experimental apparatus could not accurately simulate the conditions in the magnet, i.e. the magnetic field profile and cooling conditions of the apparatus may have increased the recovery current of the conductor [16]. It is easy to see that the evaluation of and improvement in the stability of the magnets is of great importance, even if the magnet is to operate below its recovery current. Reducing degradation in the magnet is of equally great importance in the manufacturing process.

When a magnet has been energized to an operation current above its recovery current, a disturbance in its winding might cause either a local normal zone or a quench, depending on the magnitude of the disturbance. Thus accurate evaluation of the Minimum Quench Energy (MQE) is crucial. MQE is the minimum disturbance energy inducing a local normal zone that propagates and thus causing a quench in a superconducting magnet. We studied this disturbance with respect to magnet design and construction.

Our work dealt with the helical coils of the LHD and aimed at the following:

(1) Improvement of the MQE evaluation method, which allows the estimation of a value of permissible disturbance at given conditions.

(2) Development of an advanced method for helical coil windings, which keeps degradation to the minimum.

(3) Prediction of operating conditions of the LHD helical coils.

Our goal was to improve the design criteria for superconducting magnets in large fusion devices and to describe a perspective of the successful construction and operation of the LHD helical coils.

2. Characteristics of Superconducting Helical Coils

This chapter presents the main aspects of superconducting helical coils and describes the parameters of the LHD helical coils.

2-1. Characteristics of Superconducting Magnets

2-1-1. Composite Superconductors

Superconductivity is the complete absence of electrical resistivity that occurs below a certain temperature, a certain magnetic field, and a certain current density. They are called the critical temperature T_c, the critical magnetic field H_c and the critical current density J_c, respectively. These three parameters define a critical surface, which depends on the material and manufacturing process. T_c and H_c are thermodynamic properties of superconducting materials invariant to metallurgical processing; J_c depends considerably on the processing method. A typical critical surface of NbTi is shown in Figure 2.1.1 [17]. Superconductivity prevails everywhere below this surface with normal resistivity everywhere above it.

The relation between magnetic field and temperature is presented by the following formula:

$$T_c(B) = T_c(0) \cdot \left[1 - \frac{B}{B_{c2}} \left\{ 1 - \left(\frac{T_0}{T_c(0)} \right)^2 \right\} \right]^{0.5} \tag{2.1.1}$$

where B is the magnetic flux density [T], $T_c(B)$ is the critical temperature [K] at the magnetic flux density B, $T_c(0)$ is the critical temperature [K] at B=0, B_{c2} is the magnetic flux density [T] at the upper critical magnetic field, and T_0 is the base temperature [K].

The relation between current and temperature is presented by the following formula.

$$I_c(T) = I_c(T_0) \cdot \frac{T_c - T}{T_c - T_0} \tag{2.1.2}$$

where T is the temperature [K], $I_c(T)$ is the critical current [A] at the temperature T, $I_c(T_0)$ is the critical current [A] at the operating temperature T_0. Typical values of $T_c(0)$ and B_{c2} for NbTi are 10 K and 10.4 T, respectively.

The current densities shown in Figure 2.1.1 are larger than that of conventional copper magnets; superconducting magnets reach much higher fields while the size of the magnet is smaller than that of conventional magnets, with only electrical power required for refrigeration and initiation of a current flow. In the LHD helical coil operation, the cost of electricity to perform experiments is almost 1/100 when employing superconducting magnets, compared with employing normal conductor. This is the main reason to employ superconducting magnets in the LHD. This is also the reason why superconducting magnet applications are utilized in various fields.

Superconductors before the 1960s were rather unstable, and great efforts have since been made to develop stable superconductors. Two major breakthroughs were co-processing with matrix metal for cryogenic stabilization, and development of multifilamentary conductors to suppress magnetic instability like flux jumps in superconductors. The material qualities of the superconductor such as NbTi and Nb_3Sn are also improved considerably until the present time. A great number of industrially made, reliable superconductors are commercially available today, especially for low-current, small-scale magnets.

High current conductors are necessary to perform the fusion experiments and other large-scale applications. The major reason for this is the need to keep quenching voltage within reasonable bounds. In other words, composite conductors have been developed for carrying high currents, as well as for enhancing stability. Also the LHD helical coils are wound by employing composite conductors. They typically comprise superconductor/copper matrix strands, which are twisted, and stabilizer of either aluminum or copper. Electromagnetic and thermal behavior of composite conductors is complicated, because they comprise several metals, which reveal characteristic physical properties particularly in low temperatures, and have complicated structure. Since the analysis of heat transfer and electric current transfer is rather difficult, analytical calculations, computer simulations and experimental methods have been performed to develop composite conductors.

2-1-2. Stability Theories and Criteria

In this section, we brief the theories of stabilization of superconductors. When a magnet is stable in the superconducting state, the magnetic field, current density and temperature of the conductor are controlled completely. But if a part of the conductor become the normal-state by some disturbance, it is hard to describe its temperature profile because of complicated processes in the conductor. Heat is generated by ohmic heating in the normal-state region, while it is transferred to other region of the conductor and also to liquid helium. These processes determine the temperature profile of the conductor and the profile also determines whether the region remains still superconducting-state or not. Therefore, the temperature stability or more generally thermal behavior of a conductor is crucial in magnet operation. In order to stabilize conductors thermally, several stability theories and criteria have been developed. Here we mention three stability theories, which are quite effective for magnet stabilization. They give rather conservative criteria, however they are widely accepted and used especially in large applications because of their validity. For more precise discussion of stabilization, numerical methods, which solve heat conduction and transfer equations with time-dependent ohmic equations self-consistently, will be needed, however we do not mention them here.

A. Cryogenic Stabilization

The basic concept of the cryogenic stabilization was developed chiefly by Stekly [18]. It is a non-dimensional model, which is derived from heat balance between the ohmic heating in a stabilizer and heat transfer to coolant. Figure 2.1.2 shows the basic principle of this theory. The conductor is made of a superconductor like NbTi and a stabilizer like copper. Typical figure of normal resistivity of NbTi is 6.5×10^{-7} Ωm at critical temperature 6.5 K in $B = 6$ T, while the annealed electrical copper at 4.2 K in $B = 6$ T has the resistivity of about 3×10^{-10} Ωm. These figures clearly shows that current easily flows into the stabilizer from the superconductor which is driven to normal state. In Figure 2.1.2, when some part of the superconductor is turned to normal-state by some disturbance, current shares between the superconductor and the stabilizer, then ohmic heating starts. However, if the cooling rate by the heat transfer from the surface of the conductor to liquid helium is larger than the heating rate in the conductor, the temperature becomes going down and finally the conductor returns to complete superconducting state. This criterion can be presented as the following formula.

$$\alpha = \frac{I^2}{q\beta P(\sum A_i/\rho_i)} < 1 \ , \tag{2.1.3}$$

where α is the stability factor, I is the operating current [A], q is the cooling heat flux [W/m^2], β is the proportion of wet to total surface of the conductor , P is the cooled perimeter [m], A_i is the cross section of the conductor material i [m^2], and ρ_i is the resistivity of the conductor material i [Ωm]. This criterion defines completely stable operation at any time as long as the conductors are sufficiently cooled. With the introduction of this criterion, practical applications of superconducting magnets spread to various fields.

B. Equal Area Theorem

This is a one-dimensional theory to estimate cryogenic stability. The thermal energy is balanced along the conductor, as shown in Figure 2.1.3. Heat generation and cooling are indicated by *GA/P* and *H* respectively along the conductor. This is the well-known "equal-area" theorem [19]. The heat generation depends on the resistivity of the stabilizer and the magnitude of the current which flowed to the stabilizer. Since the total current should be the same along the conductor, the heat generation is proportional to the resistivity which increases with the temperature. The cooling rate depends on the boiling condition, of which there are two types, nucleate boiling and film boiling. The cooling rate once increases with the temperature in the nucleate boiling region, but after the boiling process is turned to the film boiling, the cooling rate decreases at once and increases again with the temperature. This process has hysteresis. The boiling process depends on the surface condition of the conductor and the temperature difference between the conductor surface and liquid helium. Figure 2.1.3 shows a diagram of the heat balance and temperature along the conductor. Assuming, for simplicity, that the heat conduction coefficient of the stabilizer is constant, the thermal equilibrium of their interface is given by the following formula:

$$\int_{\theta_0}^{\theta_1} \left\{ H(\theta) - \frac{A}{P} G(\theta) \right\} \mathrm{d}\theta = 0 , \tag{2.1.4}$$

where θ is the temperature [K], θ_0 is the base temperature [K], θ_1 is the temperature of normal zone center [K], $H(\theta)$ is the cooling per unit area [W/m^2], A and P is the cross-sectional area [m^2] and the cooled perimeter [m] of the conductor. $G(\theta)$ is the heat generation per unit volume [W/m^3]. Below the current, for which $G(\theta)$ satisfies Equation (2.1.4), a localized normal zone will eventually shrink, and complete superconductivity will be restored. This current is called the recovery current of the magnet. Large magnets in power-electric use are often designed to operate below their recovery current, because of the tried validity of this criterion and because they require fewer stabilizers than if built according to the older Stekly's criterion. The criterion (2.1.4) also defines fully stable operation but in a broader sense than (2.1.3), because the complete superconductivity will always be regained as long as the conductors are sufficiently cooled.

C. Minimum Propagating Zone (MPZ)

The concept of MPZ was introduced by Wipf [20], and this is also one-dimensional estimation. Assuming a hot spot which has been produced by a point disturbance in a wire carrying its critical current density, under longitudinal heat balanced conditions, we may equate ohmic heating to heat conduction loss. A normal zone which is longer than a certain length will grow because generation exceeds cooling by longitudinal conduction. Conversely a shorter zone will collapse and full superconductivity will be recovered. This certain length can be formulated simply as following.

$$l = \left\{ \frac{2\lambda(\theta_{\rm c} - \theta_0)}{J_{\rm c}^2 \rho} \right\}^{\frac{1}{2}}, \qquad (2.1.5)$$

where l is the length of minimum propagating zone [m], λ is the thermal conductivity [W/mK], $\theta_{\rm c}$ is the critical temperature [K], θ_0 is the base temperature [K], $J_{\rm c}$ is the critical current density [A/m^2], and ρ is the normal state resistivity [Ωm]. Equation (2.1.5) is often used to characterize the stability of superconducting magnets.

2-1-3. Minimum Quench Energy (MQE)

Once the conductor is driven normal by some disturbance, there is a certain current below which superconductivity is restored. This current is called as its recovery current. Below the recovery current, some disturbance can only cause a localized normal zone but cannot cause a quench. On the other hand, above the recovery current, some disturbance which can cause a localized normal zone immediately causes a quench. Therefore, above the recovery current, minimum disturbance energy which causes a localized normal zone can be defined as the minimum quench energy (MQE). At its critical current, of course, no disturbance energy is needed to cause transition to the normal state.

In this thesis, we will use the concept of MQE as one of crucial indices to characterize magnet stability. Furthermore, even below the recovery current, we will also use the term MQE to present the energy which cause a localized normal zone. It may seem stretching the meaning of the term, however the essential phenomena before quenches are the same in spite of the transport currents, thus we dare to do so. In Chapter 3, MQE near a recovery current will be investigated experimentally and analytically.

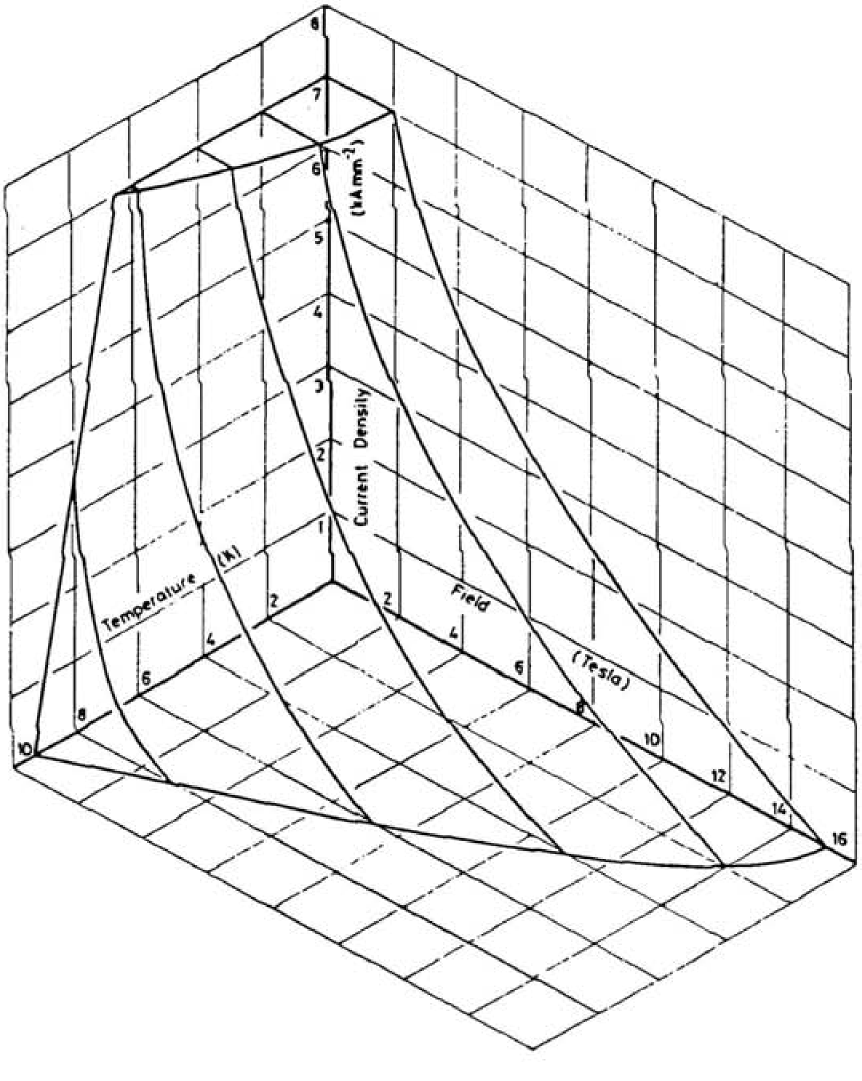

Figure 2.1.1 Critical surface for a commercial superconducting alloy of niobium-titanium. Superconductivity, i.e. complete absence of electrical resistivity, prevails everywhere below this surface with normal resistivity everywhere above it [17].

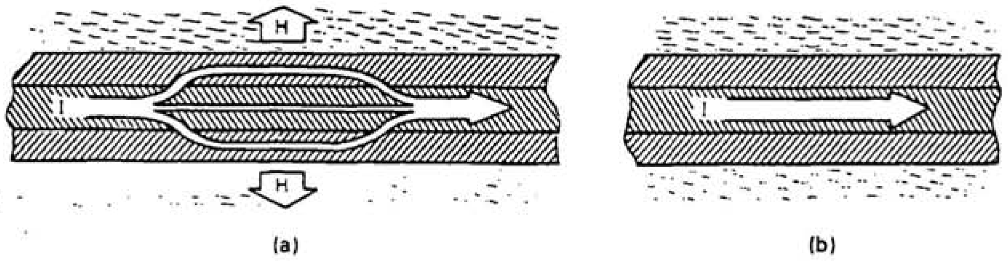

Figure 2.1.2 (a) Cryogenic stabilization; following a disturbance current shares between the stabilizer and the superconductor; ohmic heat generation is transferred to the coolant; (b) if the available cooling exceeds heat generation, temperature falls and current returns to the superconductor [17].

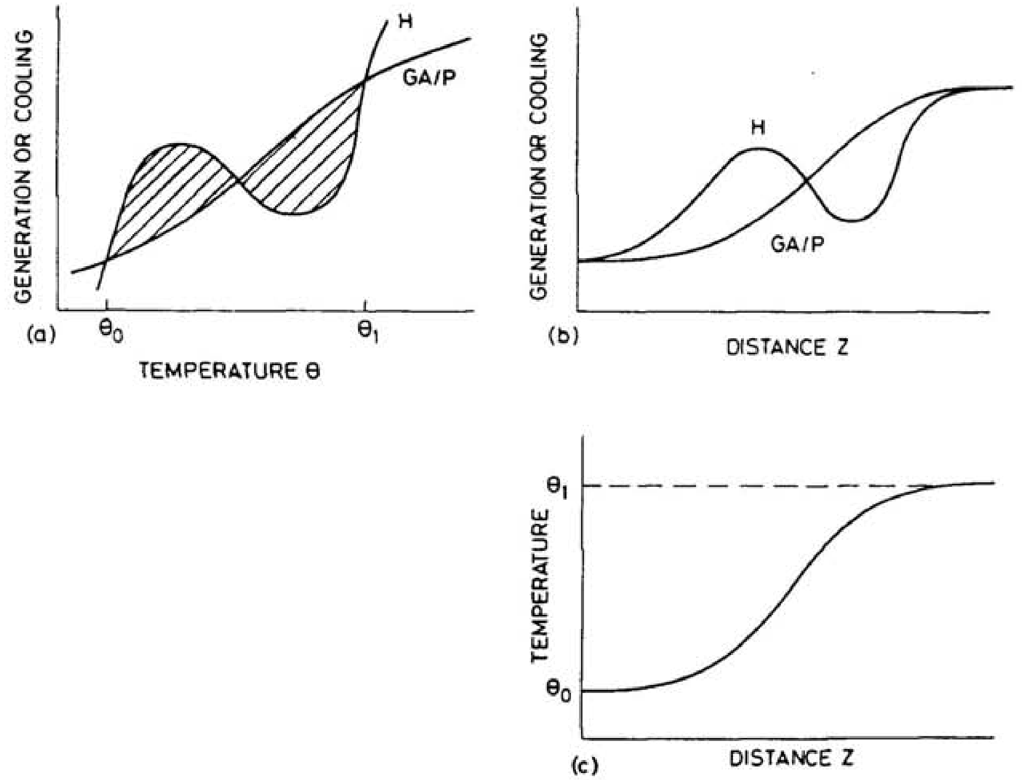

Figure 2.1.3 Variation of temperature, heat generation, and cooling along a heat-generating bar with arbitrary $G(\theta)$, immersed in a coolant with arbitrary heat transfer $H(\theta)$ [17]. Equal-area theorem can be translated into the simple geometrical interpretation that no net area should be enclosed between the generation and cooling curves, i.e. the two shaded areas in (a) must be equal.

2-2. Characteristics of Helical Coils

2-2-1. Geometrical Characteristics

Geometrical loci of helical coils are designed in accordance with the optimization of magnetic field profile. In the continuous winding system, helical conductors are wound on a torus according to loci equations. An example of loci equations of helical coils is

$$\theta = -\{(m/l)\phi + \alpha\sin((m/l)\phi)\} \tag{2.2.1}$$

where θ is the poloidal angle, ϕ is the toroidal angle, α is the pitch modulation parameter, l is the poloidal period number, and m is the toroidal period number [21]. Equation (2.2.1) and a major radius R_c and a minor radius a_c of a coil determines its geometrical locus.

In Equation (2.2.1), a positive pitch modulation results in a large, clear outermost magnetic surface because it compensates the discrepancy from the helical symmetry due to the toroidicity. Thus, the positive pitch modulation enhances the clearance between the plasma surface and the vacuum vessel wall. On the other hand, a negative pitch modulation will result in improvement of plasma transport, since the magnetic ripple in the weak field strength region decreases [22]. These factors make it difficult to determine the optimum pitch modulation parameter from the viewpoint of both the plasma performance and engineering feasibility. In LHD, the pitch modulation parameter was decided as $\alpha = 0.1$ with $l = 2$, $m = 10$, $R_c = 3.9$ m and $a_c = 0.975$ m to satisfy these conflicting demands.

From the viewpoint of fabricating helical coils, it is preferable that each locus is a geodesic line on the torus, because geodesic line makes possible to wind conductors with tension, which is effective for precise fabrication of coils. On the torus surface, torus effect makes loci contorted, even when they have no pitch modulations. If a coil bobbin is only a simple cylinder, not a torus, the loci with no pitch modulations would be simple helical lines, i.e. geodesic lines on the cylinder. Even on the torus surface, some pitch modulations which compensate the torus effect make the loci geodesic lines. They can be presented as summations of sine function series, however, such loci do not generally meet the requests to helical coils from the plasma performance of a fusion experimental device. As a result, the loci on the torus, shown as Equation (2.2.1), are compelled to be non-geodesic lines, so they have two curvatures and torsion. Especially one of these curvatures give some engineering difficulty in fabricating coils. A method and an outcome of overcoming this difficulty are described in Chapter 4.

2-2-2. Helical Coils of the Large Helical Device (LHD)

As is mentioned in Section 1-1., the Large Helical Device (LHD) is now under construction at Toki, the new site of the National Institute for Fusion Science (NIFS) of Japan. In this section, we will review the specifications of the LHD helical coils as the introduction to the following chapters.

The helical coils are the pool-cooled superconducting coils which are designed to satisfy the criterion for full stabilization in a broad sense i.e., Maddock's equal area theorem [19]. Major parameters of the helical coils are listed in Table 2.2.1 [23]. A cross-sectional view of the helical coils is shown in Figure 2.2.1, and a diagram of a part of the helical coils is shown in Figure 2.2.2. Specifications of the conductor of the helical coils will be described in detail in section 3-1. The conductor consists of NbTi/Cu compacted strands, a pure aluminum stabilizer with Cu-2%Ni clad, and a half-hard copper sheath. Since they are not able to bear large electromagnetic force in operation by themselves, they are designed to be packed into a thick non-magnetized alloy case which is also used as both of a bobbin for winding and a bath for liquid helium. Ground insulation was directly stuck on the inner surface of the can and cured by the autoclave method which was specifically developed for these coils. The conductors are directly wound on the can from its bottom with 450 turns per one coil , and the total length of the conductors will be 36 km in two coils. GFRP electrical insulators are settled at intervals between the conductors to arrange cooling channels for liquid helium.

In the phase I operation of LHD, the helical coils are cooled with saturated liquid helium at 4.4 K. They are designed to be fully stabilized; their designed recovery current exceeds its rated current. The measured recovery current of the conductor was 13.0 kA, with conductor samples at the proportion 0.5 of wet to total surface, in 4.4 K and 7 T in the test facility, which will be described in the next chapter. The proportion of wet to total surface in the helical coils was finally optimized in the range from 30% to 70% depending on each turn and each position along the conductors [24]. Thus the recovery current of the helical coils is calculated to be 15.0 kA at 4.4 K and 7 T. An advanced cooling with superfluid helium is planned for higher magnetic fields in the phase II operation.

Coil winding accuracy in its manufacturing process is one of the most crucial factor to achieve the objectives of this device. As well as assuring its magnetic profiles, satisfying design criteria on mechanical strength is the most important for its operations. If its winding accuracy is poor, it causes to lessen the mechanical rigidity of the helical coils as the assemblies of the conductors. In operations of the LHD, the helical coils as the assemblies of the conductors will be moved in the coil can by the electromagnetic force; they are stretched along the conductors and compressed in its cross-sectional plane. The winding accuracy criterion which is determined from the yield strength of the conductors is control of gaps below 65 μm per each layer. It has been achieved so far in on-site winding of the helical coils [23].

In the next chapter, the stability of the helical coils will be discussed from a viewpoint of MQE, which was previously defined in the section 2-1. Also a development of a manufacturing method which aimed to satisfy severe requirements in its winding accuracy will be described in Chapter 4.

Table 2.2.1 Major parameters of the helical coils [23]. In the phase I operation, the helical coils are cooled with saturated liquid helium at 4.4 K. An advanced cooling with superfluid helium is planned for higher magnetic fields in the phase II operation.

item	Phase I	Phase II
Bath Temperature	~ 4.4 K	~ 1.8 K
Central Toroidal Field	3 T	4 T
Maximum Field in Coil	6.9 T	9.2 T
Nominal Current	13.0 kA	17.3 kA
Recovery current (cal.)	15.0 kA	–
Current Density	40 A/mm^2	53 A/mm^2
Magnetic stored energy	0.92 GJ	1.64 GJ
Voltage to earth	±1181 V	±1574 V
Voltage between layers	393 V	525 V
Major Radius/Minor Radius	3.9 m/0.975 m	
Superconductor	Al stabilized NbTi/Cu	
Surface treatment	Oxidization	
Number of Turns	450	
Size of conductor	12.5 mm×18.0 mm	
Spacer factor	30%~70%	
Spacer pitch	49.2 mm~64.3 mm	

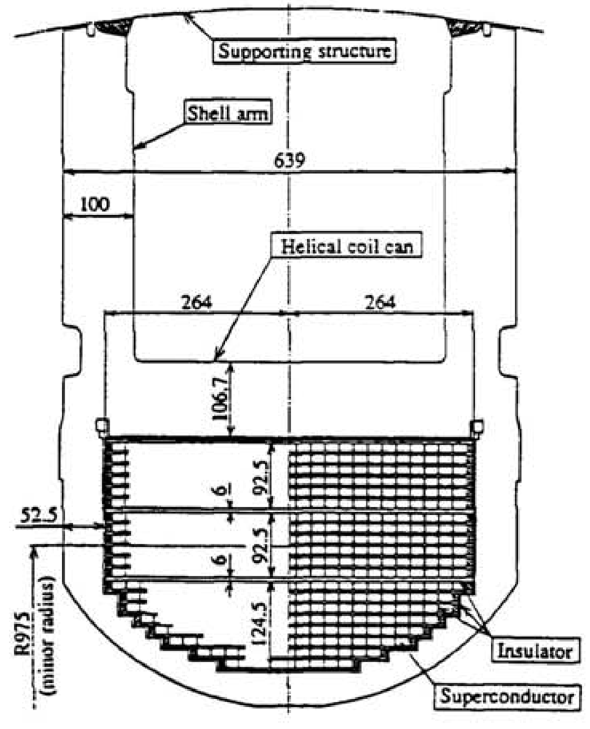

Figure 2.2.1 Cross-sectional view of the helical coil [23]. Each one of the pair of helical coils is supported by a large, torus-shaped structure. Each helical coil contains 450 conductors windings, 900 in all, and their total length is 36 km in the two coils. The coil cans are made of non-magnetized thick steel, which withstands strong electromagnetic force. The coil cans also serve as bobbins for the windings and baths for the liquid helium. During energization, the helical coils and the supporting structure are cooled to the temperature of liquid helium.

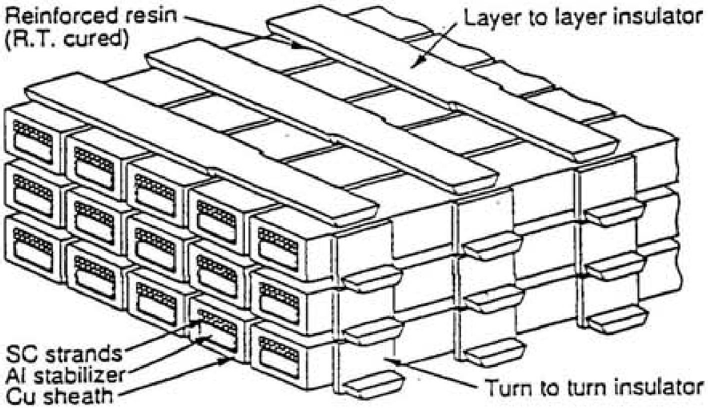

Figure 2.2.2 Diagram of a part of the helical coil windings [23]. The conductors are assembled with slat-shaped GFRP insulators between each turn. This configuration provides enough cooling for superconductors with liquid helium. The proportion of wet to total surface of the conductor varies with the position in the coil to improve the cooling rate and satisfy the mechanical strength requirements of the coil materials.

3. Analysis of the Thermal Behavior of Superconductors

3-1. Superconductor Performance Test

3-1-1. Experimental Facility

For the evaluation of conductor performance for large magnets, a conductor test facility has been available in the National Institute for Fusion Science. The conductor which is the subject of this thesis has also been tested at this facility [25]. Its major part consists of a pair of 100 kA current leads, a pair of maximum 9 T background split coils and a cryostat as shown in Figure 3.1.1. They are accompanied with a 75 kA DC power supply and a measurement system. Figure 3.1.2 shows a schematic drawing of a sample for the conductor performance tests [26]. It consists of a pair of U-shaped copper block leads, a pair of short conductors which were soldered together at the bottom, and a triangle-shaped GFRP block for positioning in the split coils. A number of GFRP spacers of 20 mm in length were arranged regularly along the conductors and provided 50 % exposure rate at the standard tests. The sample also had many voltage taps to measure its normal state resistance and normal zone propagation velocity. Thermocouples and thermometers were also attached to measure its temperature rise after the transition to a normal state. They were installed beneath the GFRP spacers, so that the predetermined exposure rate of the conductor would not change. The sample was inserted vertically into the aperture of the split coils. A profile of the generated magnetic field is shown in Figure 3.1.3. It has a 90 % flat top region of about 250 mm along the sample conductors. A self magnetic field was incorporated into evaluation of each measurement.

It should be noted that the characteristics of this apparatus may affect on measured performance of the conductors. Plentiful liquid helium makes a better cooling condition than in real magnets, and the limited flat top region of the magnetic field prevents the normal zone from propagating. Using this type of facility, therefore, the conductors are sometimes in a different, often better, atmosphere from a viewpoint of stability than in the magnet for which the conductors are really assembled. Those differences have to be incorporated into the evaluation of conductor performance.

3-1-2. MQE Measurement by Simulated Disturbance

In the facility described in the previous section, several candidates for the conductors for the LHD helical coils were tested, and the conductor which is named KISO-32 was selected. This thesis deals with this actual conductor.

Figure 3.1.4 shows the cross section of the KISO-32 conductor. Its major parameters are listed in Table 3.1.1 [27]. Its dimension is 12.5 mm × 18.0 mm, and its rated current is 13 kA at 7 T. It consists of NbTi/Cu compacted strand cables and a pure aluminum stabilizer side by side, and a Cu sheath around them. Cu-2%Ni is used as the cladding material around the aluminum stabilizer to reduce the anomalous magnetoresistivity by the Hall effect [28]. The surface of the conductor is coated with copper oxide to enhance the heat transfer from the conductor surface to the liquid helium in the film boiling region [43].

We measured the items as follows: critical currents, recovery currents from their normal states, and some other parameters concerned with stability margins. The critical current evaluation was described by Mito, et al.[25], and recovery current characteristics were discussed by Yanagi, et al.[26] and Imagawa, et al.[29]. Figure 3.1.5 shows the measured recovery current of R&D conductors including KISO-32 under external magnetic fields of 3 T to 7.5 T. Its horizontal axis shows external magnetic fields produced by the split coils, and its vertical axis shows measured recovery currents. The value of the external magnetic fields were determined by considering that the conductors in real helical coils will experience the maximum field of 7 T when the field at plasma center is set at 3 T, which is one of the standard operation parameters at phase I. Each recovery current was observed at which entire superconductivity was restored when decreasing the current of the conductor after the transition to a normal state which we generated by heaters. Open circles in Figure 3.1.5 indicates the performance of KISO-32 which was subjected to the external magnetic field parallel to 18 mm side of the conductors. Open triangles and open squares indicate the performance KISO-32 and KISO-33 respectively, under the field parallel to 12.5 mm side. In real helical coils, conductors in their maximum field are mainly subjected to the field parallel to 18 mm side, so the open circles can be regarded as the conductor performance when the conductor is installed in the real helical coils.

One of the necessary conditions of conductors is that the values of their recovery currents prevail the rated current at phase I, 13.0 kA at 7 T. Open circles, which represents the conductor performance in early stage of the production of the same type, meet this requests. Subsequent same-type conductors have also met this requests successfully.

In every experiment routine, along with the measurements of critical currents and recovery currents, we measured the stability margins of conductors. We needed to initiate a transition to a normal state investigate the stability margin, and then we used the resistive heater which was attached to the conductor at the center of the external magnetic field. The resistive heater was composed of a stainless steel tape with a polyimide surface insulation, and was non-inductively wound around the conductor. The dimensions of the heater materials depended on conductor samples; their typical thickness of stainless steel tapes and polyimide insulations was 0.1 mm, respectively. Figure 3.1.6 shows a schematic view of the heater which is used in this experiment. The heater was installed beneath the GFRP spacer as other measurement taps to simulate the frictional disturbance in the actual coil and not to change the exposure rate. A schematic view of its installation is shown in Figure 3.1.7. We observed whether a localized normal zone was generated or not and whether it propagated depending on the magnitude and the duration of the simulated disturbances. Figure 3.1.8 shows example wave forms of the voltage which were observed when the normal zone induced by the external heat pulse. When a rather short duration's heat pulse which had the power large enough to cause propagating normal zone was inputted, shown in (a), a quenching occurred immediately. In this example the voltage, which emerged through the current flowing to the stabilizer, along the conductor increased rapidly; it meant the rapid propagation of a normal zone, so the current was shut down soon. As shown in (b), with a rather long duration pulse, which had the power not large enough to cause the transition to a normal state immediately, a quenching occurred often during the pulse. It is due to the delay time of temperature rise caused by the balance between energy input by the heater and energy dissipation by heat transfer to liquid helium and heat conduction along the longitudinal direction of the conductor.

Figure 3.1.9 shows an example of measured MQE versus pulse duration. Each open circle indicates MQE, in practice the maximum value of input energy when a normal zone stagnated or shrunk after a localized normal zone was deliberately caused by the heat input, at each duration of pulses. Each open triangle indicates the value of input power corresponds to each MQE. Pulse duration was varied from 10 millisecond to 1 second. Its shorter limit is determined to simulate real disturbances in magnets as much as possible. Its longer limit is determined to simulate time-integrated numerous disturbances occurring continuously in real magnets. Durations of disturbances in real magnets are reported as below 1 millisecond [30] per one phenomenon, so we have to say our shorter limit is still longer than the one in real magnets. However, using a large conductor and a heater adjusted in size to the conductor compelled prolongation of their time constants in measurements. The time resolution of the measurement system is about 10 ms.

In Figure 3.1.9, the measured MQE, denoted as open circles and a solid line, decreases as the pulse duration decreases, then converges to a constant value. This constant value has been regarded as the MQE at given magnetic field and transport current. From the viewpoint of power, its value decreases as the pulse duration increases, shown as open triangles and a dotted line. It is due to that the energy dissipation rate during heating increases as pulse duration increases. In practical use, the converged value of energy has much more importance than that of power, because real disturbances probably have short durations below 1 ms.

It should be noted that the duration value at which the measured MQE begin to converge is a few ten milliseconds. It is much larger than the duration value of real disturbances, and also is considered to be dominated by the time constant of this type of measurement. Therefore, the measured MQE by the method above might be overestimated. Seo, et al. [31] investigated the pulse duration dependence of MQE by using a specifically designed carbon paste heater, which has a much smaller heat capacity than other resistive heaters'. Figure 3.1.10 shows one of their results. It shows that the measured MQE by utilizing the carbon paste heater is smaller by one order than the MQE value by utilizing a resistive heating wire. Their method is effective, however, that type of heater is frail and is lacking in reproducibility. It is also difficult to apply to such conductors as KISO-32 which have a much larger size than their conductor and are also subjected to severe tests with large currents. We investigated another method equivalent in its effect to utilization of the heater of which the heat capacity is small enough for MQE measurements. It is described in detail in the next section.

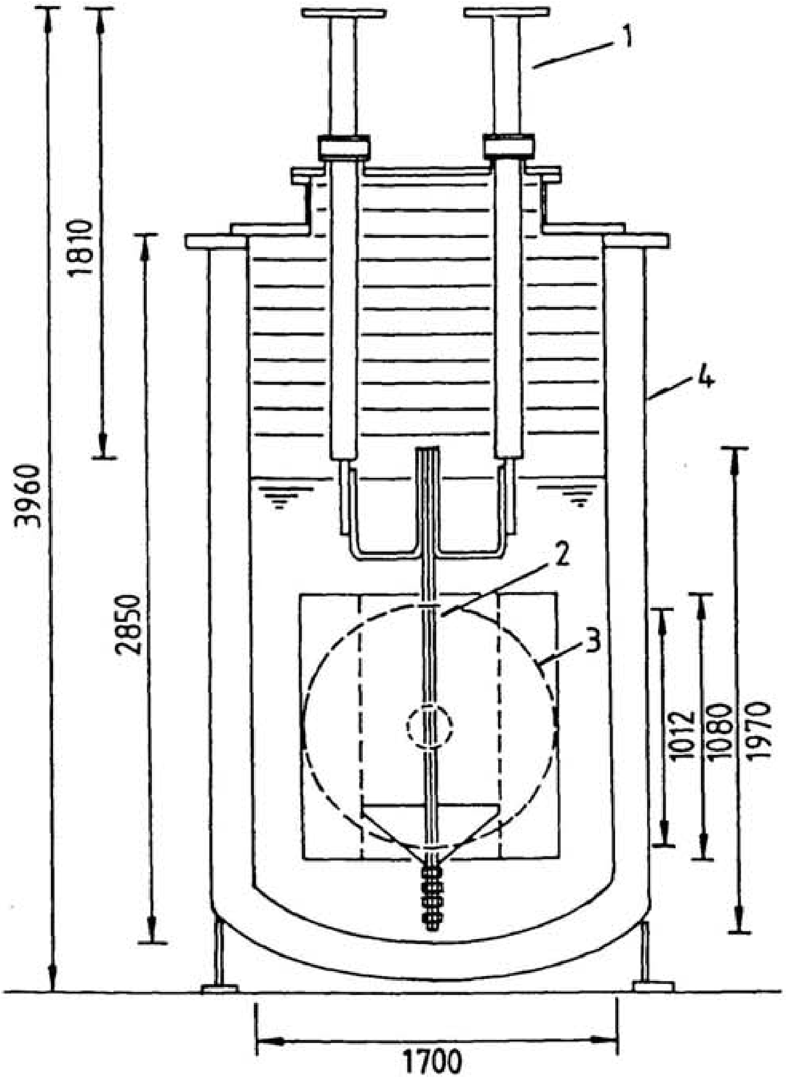

Figure 3.1.1 Cross-section of the conductor test facility, (1) 100 kA current leads, (2) Sample conductors, (3) Background split coils, (4) Cryostat [25]. The background split coils produce magnetic fields up to maximum 9 T for providing the magnetic atmosphere of real magnets. Conductor samples are inserted vertically into the split coils, and subjected to liquid helium and the external magnetic fields.

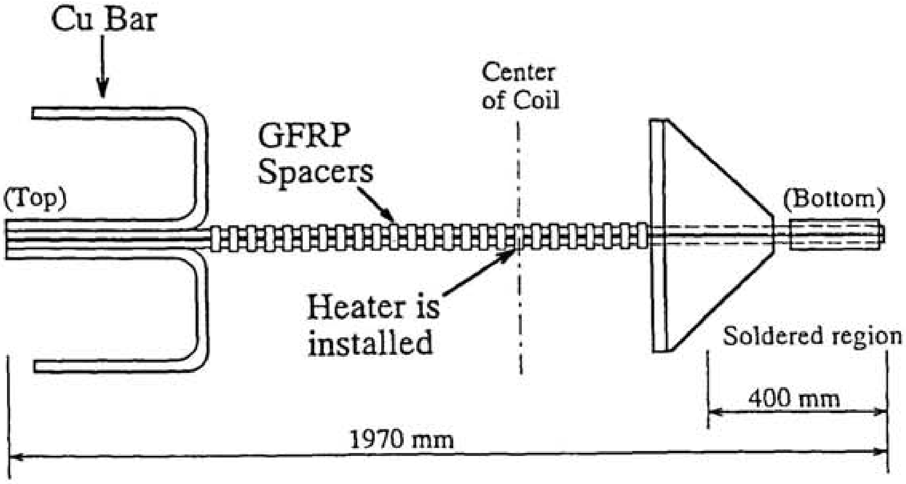

Figure 3.1.2 A sample for the conductor performance tests. Two conductors are soldered together at the bottom. A number of GFRP spacers of 20 mm in length are arranged regularly along the conductors and provided 50 % exposure rate at the standard tests. The sample also have many voltage taps and thermometers. Simulated disturbances are caused with a resistive heater attached at the center of the coil. The sample is inserted vertically into the aperture of the split coils [26].

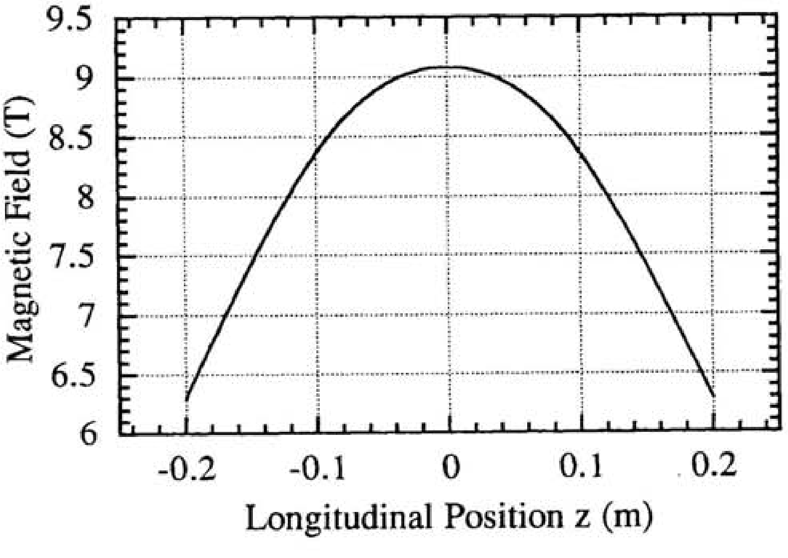

Figure 3.1.3 Magnetic field profile of a pair of split coils. It has a 90 % flat top region of about 250 mm along sample conductors.

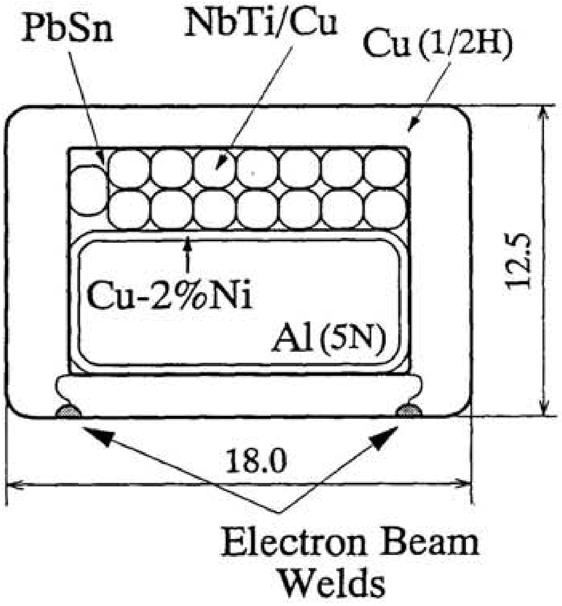

Figure 3.1.4 Cross-section of KISO-32 conductor [27]. It consists of NbTi/Cu compacted strand cables and a pure aluminum stabilizer side by side, and a Cu sheath around them. Cu-2%Ni is used as the cladding material around the aluminum stabilizer to reduce the anomalous magnetoresistivity by the Hall effect.

Table 3.1.1 Major parameters of KISO-32 conductor [27].

Conductor Size	12.5 mm x 18.0 mm
Superconducting Material	NbTi
Copper to NbTi ratio	0.9
Diameter of Filaments	47 μm
Number of Filaments	726
Diameter of Strand	1.74 mm
Number of Strands	15
Critical Current Density at 7T, 4.4K	1360 A/mm^2
Resistivity of Aluminum at 7T, 4.4K	3.8×10^{-11} Ωm
Nominal Current at Phase I	13.0 kA
at Phase II	17.3 kA

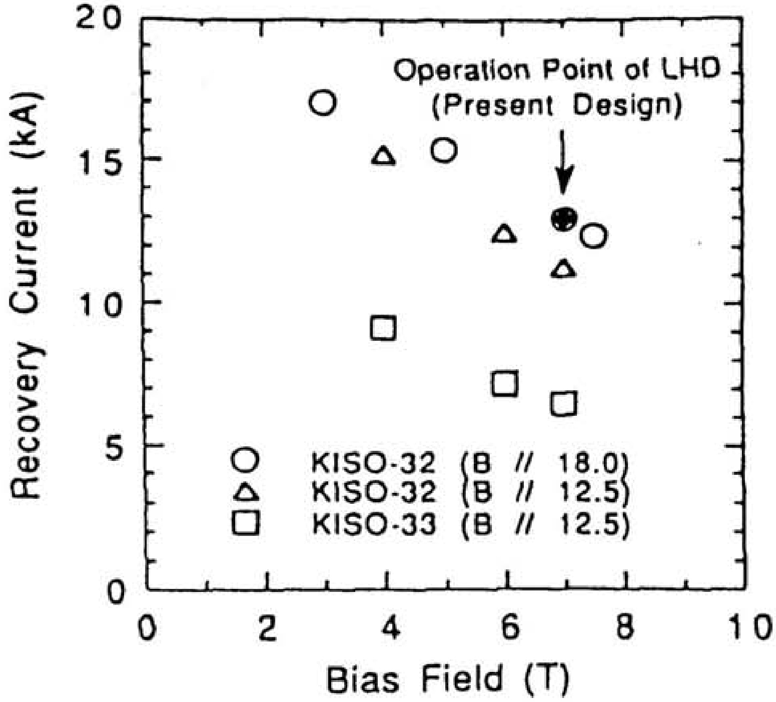

Figure 3.1.5 Measured recovery current of KISO-30 series conductors. B//18.0 (12.5) means the condition when the external field was parallel to the 18.0 (12.5) mm surface [26]. Each recovery current was observed at which entire superconductivity was restored when decreasing the current of the conductor after the transition to normal state which was induced with heaters. In real helical coils, conductors in their maximum field are mainly subjected to the field parallel to 18 mm side, so the open circles can be regarded as the conductor performance when the conductor is installed in the real helical coils.

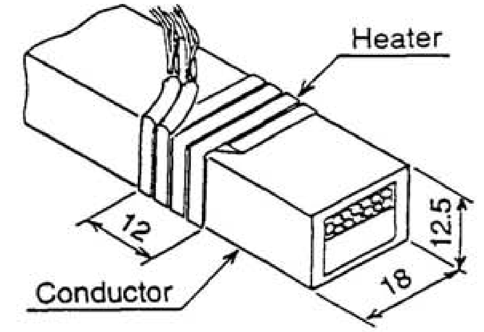

Figure 3.1.6 Schematic drawing of heating device for simulated disturbances. The heater is wound around the conductor non-inductively. The heater is composed of the stainless steel tape coated with polyimide insulation. Thickness of the stainless steel tape and the polyimide insulation was 0.1 mm, respectively.

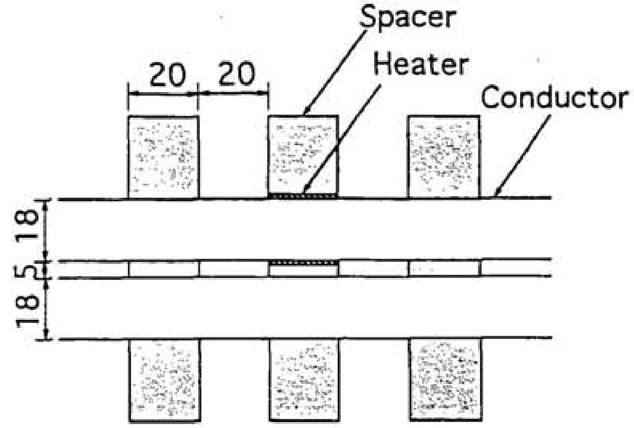

Figure 3.1.7 Schematic drawing of heater installation. The heater was installed beneath the GFRP spacer as other measurement taps to simulate the frictional disturbances in the actual coil and not to change the exposure rate of the conductor.

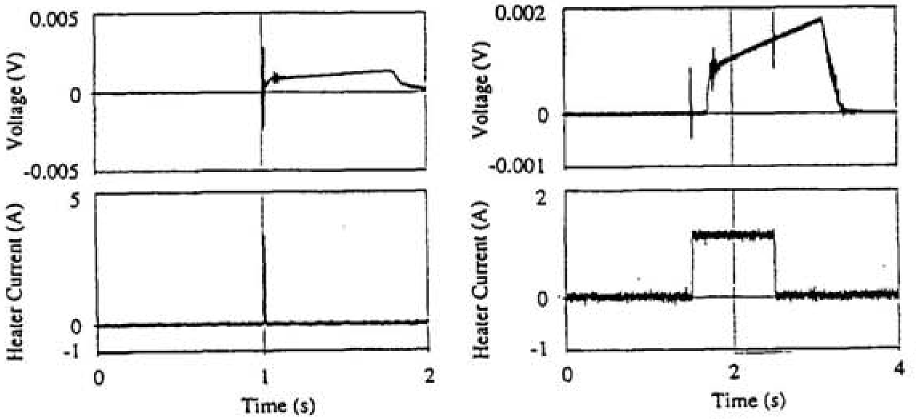

(a)

(b)

Figure 3.1.8 Time evolution of sample voltage when a heat pulse of (a) 10 ms or (b) 1 s is applied to a conductor. Observed increase in the voltage indicates a propagation of a normal zone.

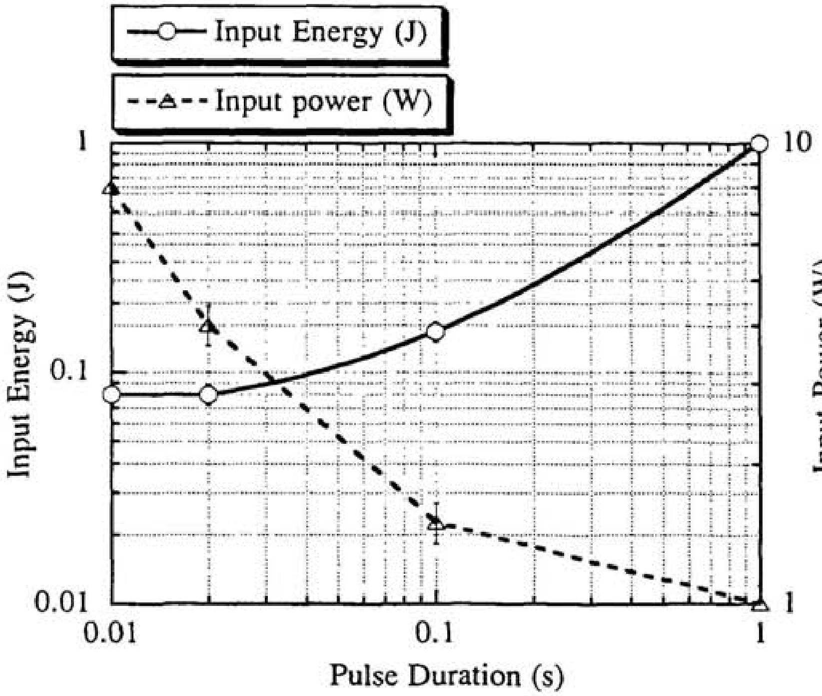

Figure 3.1.9 Dependence of minimum input energy to cause quenching on pulse duration. The measured MQE, denoted as open circles and a solid line, decreases as the pulse duration decreases, then converges to a constant value. This constant value has been regarded as the MQE at given magnetic field and transport current. Triangles and a dotted line denote the power needed to cause quenching.

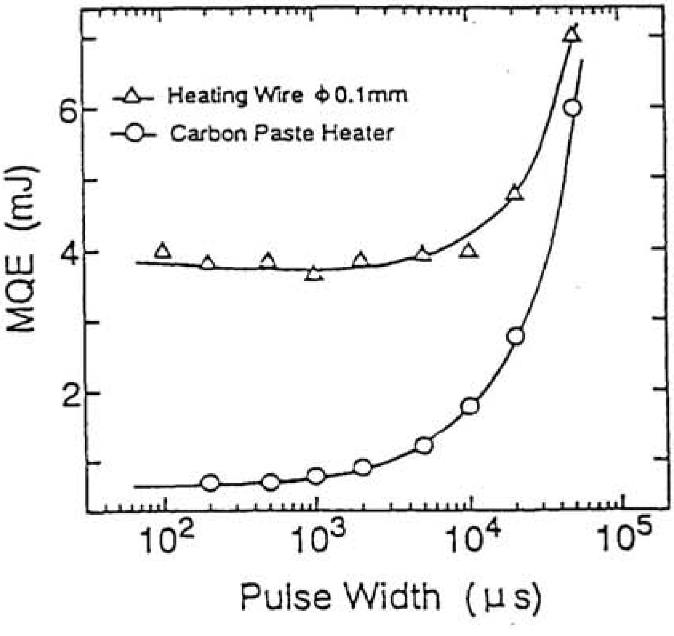

Figure 3.1.10 Pulse width dependence of MQE when carbon paste heater is used. MQE become one order smaller than the value obtained by a conventional resistive heater [31].

3-2. Heating Efficiency under Simulated Disturbances

3-2-1. Two-Dimensional Analysis Model

In order to estimate MQE more precisely, we tried to estimate the net input energy into the conductor by using thermal analysis. For simplicity, we calculated heat transfer in a cross-section of the conductor including the heater two dimensionally. We employed a widely-used finite element method computer code (ADINA™). Thermal analysis at low temperature is generally accompanied by difficulties in solution convergence, partly because the physical properties of each of the materials in analysis meshes are significantly different from each other. In addition they each have an inherent dependence on temperature, and also in part, the aspect ratios of some meshes are inevitably large owing to the shapes of the materials. We avoided those problems by devising a way to create the meshes.

In this model, heat pulses are assumed to be supplied at the heater around the conductor as in the experiments. As a boundary condition, it was assumed that the surface of the heater was cooled by liquid helium through adjacent cooling channels. This may be applicable when thermal conductivity of the conductor surface material is large enough. Although our experiments and analyses dealt with transient phenomena, the heat transfer coefficient was set at a constant value of 5 $kW/m^2 \cdot K$, which is the value at steady-state nucleate boiling. The reason we used this value was because the temperature rise of its adjacent exposed conductor surface was considered to be not large enough to cause transient heat transfer, though the temperature rise of polyimide insulation reach several Kelvin. Steward investigated the transient heat transfer in liquid helium, and established a diagram which describes time evolution of boiling manner and temperature rise on the surface of heated substances immersed in a saturated liquid helium [32]. His diagram shows that in the case where the temperature rise ΔT is smaller than 1 K, heat transfer coefficients below a certain value, which is typically 6 kW/m^2, are almost constant along time evolution. Hence, on the assumption of small temperature rise ΔT of the conductor surface, we can use a value at steady-state nucleate boiling even in a transient phenomenon.

Thermal properties of each of the materials in the analysis mesh were set to be dependent on temperature.

Under these conditions, the temperature variation of all materials was calculated for several types of input pulse to the heater.

3-2-2. Results of Temperature Variation

Figure 3.2.1 shows the result of a calculation for a relatively short (0.01 s) pulse with high power (8 W) in our experiment conditions. The temperature of the NbTi filament exceeds the current sharing temperature T_{CS} near the end of the pulse. It shows a good agreement with the time when voltage signal was observed in our experimental results. Figure 3.2.2 shows the result at relatively long (0.1 s) pulse with low power (1.5W) in our experiment conditions. It shows a remarkable temperature rise at each material, and the temperature of NbTi exceeds T_{CS} at an early stage of heating in contrast to our experimental results. This analysis may contain some errors particularly for longer pulses because this two dimensional model does not include heat conduction along the conductor. In other words, energy dissipation rate is lower than that in the actual phenomena, then the temperature rise becomes steeper. However, this analysis agrees well with the result of short pulse experiments, which simulates actual disturbances more correctly, because the effect of heat conduction is negligible. We will consider a distribution of input energy among conductor materials with the procedure described in the next section.

3-2-3. Energy Distribution and Heating Efficiency

In order to estimate net input energy into each material in the conductor and the heater, we calculated the stored energy in each material i using the following equation:

$$E_i(t)=\int_0^t M_i C_i(T_i)\frac{\mathrm{d}T_i}{\mathrm{d}t}\mathrm{d}t \ , \tag{3.2.1}$$

where E_i is the stored energy in each material, M_i is mass, C_i is heat capacity, and T_i is the temperature of each material.

Heat transfer to liquid helium can be estimated in the same way:

$$E_h(t)\approx\int_0^t Sh(T_P)(T_P-T_0)\mathrm{d}t \ , \tag{3.2.2}$$

where E_h is energy transfer to liquid helium, S is heat transfer area, h is the heat transfer coefficient, T_P is the temperature of heater surface, and T_0 is the temperature of the helium bath.

By using (3.2.1) and (3.2.2) we acquire the time dependence of energy distribution in each of the materials:

$$R_i(t)=\frac{E_i(t)}{\sum\limits_i E_i(t)+E_h(t)} \ . \tag{3.2.3}$$

Summation is taken over all materials of the conductor and the heater. The denominator of (3.2.3) should be equal to the total input energy to the heater until time t.

Figure 3.2.3 shows the calculated time dependence of energy distribution of each material corresponding to the case of Figure 3.2.1. It shows that conductor materials receive energy less than 10% of all input energy. It also shows that since heater materials have large heat capacities and low thermal conductivities, they tend to store thermal energy in themselves in shorter pulse conditions. Figure 3.2.4 shows the time dependence of energy distribution of each material corresponding to the case of Figure 3.2.2. In this case, energy transfer to liquid helium is considerably larger compared with the case of Figure 3.2.1. It also shows that conductor materials receive less than 10 % of all input energy. These results show that considering the experimental total input energy to be its stability margin may be overestimation, while estimating the net input energy by thermal analysis will be helpful in assessing the real stability margin.

We estimated the net input energy into the conductor materials in stability margin experiments by a two-dimensional thermal analysis. The results show that conductor materials received energy less than 10% of all input energy regardless of the pulse durations, when conventional resistive heaters were used. It shows good agreement with the study by Seo, et al.[31] in its tendency. Our estimation method will be helpful in assessing the real stability margin for larger size conductors like in this experiment, where applying heater pulses, as short as duration of actual disturbances in real magnets, is difficult.

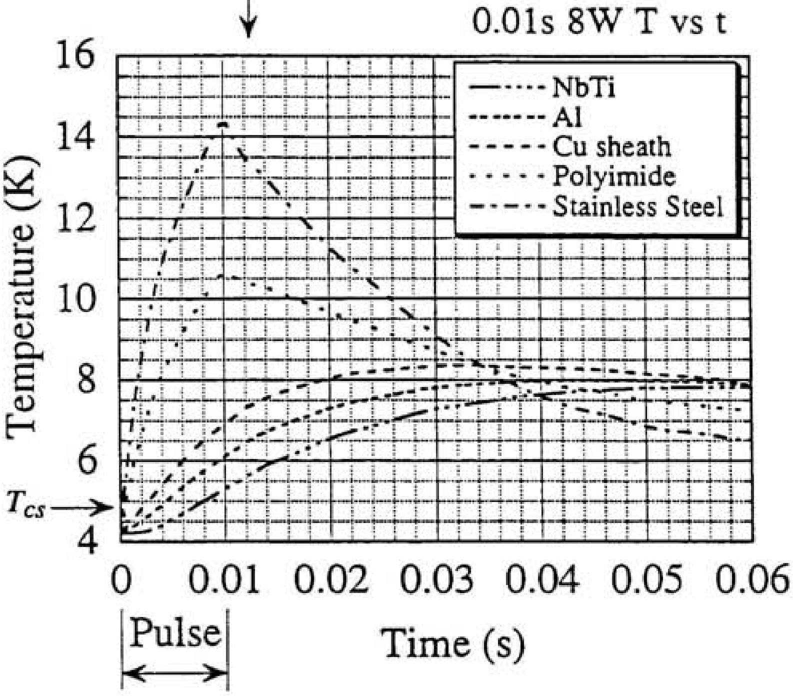

Figure 3.2.1 Calculated temperature variation when the heat pulse of 0.01 s (8W) is applied. Quenching occurred at 0.0125 s, i.e. just after the end of the pulse. The temperature of NbTi reach the current sharing temperature T_{cs} at the end of the pulse.

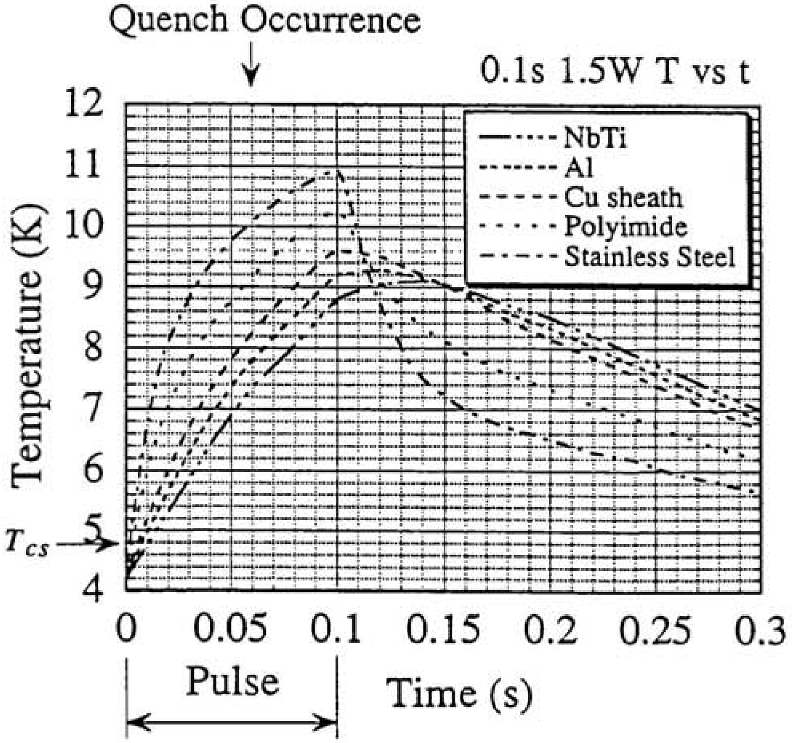

Figure 3.2.2 Calculated temperature variation when the heat pulse of 0.1 s (1.5W) is applied. Quenching occurred during the pulse. The temperature of NbTi reach the current sharing temperature T_{cs} at the beginning of the pulse.

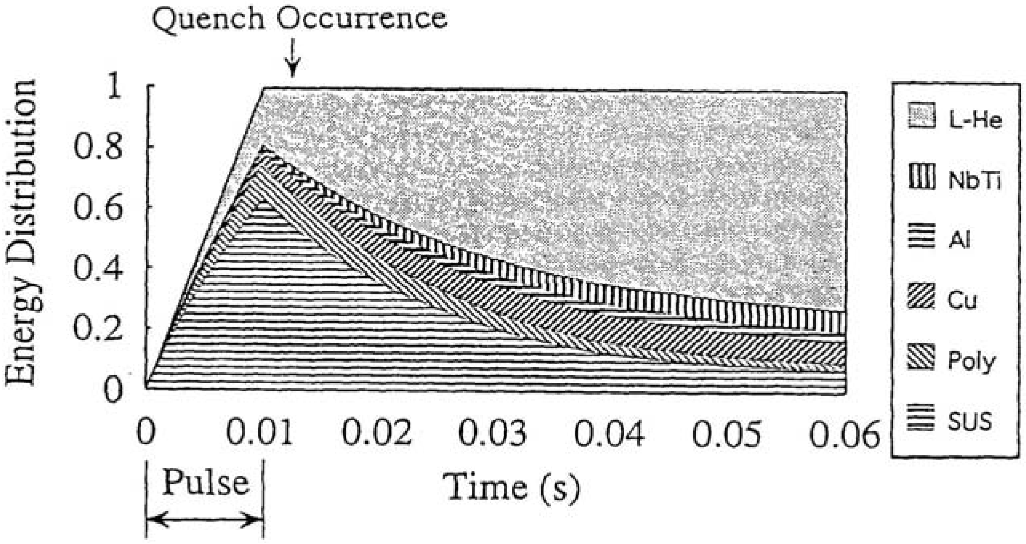

Figure 3.2.3 Time evolution of energy distribution of each material corresponding to the case of Figure 3.2.1. Quenching occurred at 0.0125 s. When the quenching occurs, Only 10% of total input energy is supplied to the conductor, which is composed of NbTi, Al, and Cu.

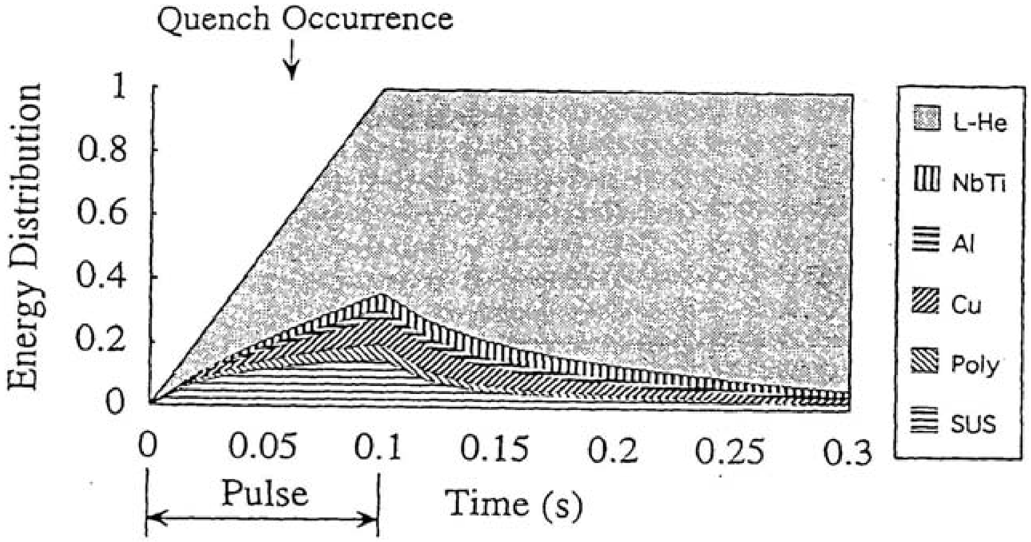

Figure 3.2.4 Time evolution of energy distribution of each material corresponding to the case of Figure 3.2.2. Energy dissipation into L-He is considerable.

3-3. Thermal Anisotropy of a Conductor

Geometrical anisotropy of a conductor cross section indicates the possibility of anisotropy in its stability margin; the stability against thermal disturbances possibly depends on the direction of heat flux to the conductor. In addition, it is considered that thermal disturbances are not uniformly distributed around conductors in real magnets, because electromagnetic force has inevitably biased distribution in real magnets. If the actual thermal disturbance occurs at a weak side of the conductor in its stability, a transition to normal state will more easily occur than is expected based on our knowledge of its stability, which is generally defined without considering the effect of anisotropy.

As our conductor KISO-32 has also a geometrical anisotropy in its cross section, it is important to investigate the anisotropy in its stability margin.

3-3-1. Anisotropic Stability Margin

In order to investigate an anisotropy in conductor's stability margin, we carried out the measurements in which heat pulses are applied to the respective sides of the conductor. Three resistive heaters were installed to three separate sides of the conductor as following:

(1) Top surface, which is adjacent to the NbTi/Cu strand

(2) Side surface, which is adjacent to the sides of NbTi/Cu strand and Al stabilizer with Cu-2%Ni clad

(3) Bottom surface, which is adjacent to the Al stabilizer with Cu-2%Ni clad.

Figure 3.3.1 shows a schematic view of arrangement of the heaters in this experiment.

Stability margin measurement was carried out in the same manner described in the previous section. Figure 3.3.2 shows a result, which clearly indicates that stability margin against heat flux from (1) direction is one third of that from (3) direction regardless of pulse duration.

Stability margin ratio of (1) side to (3) side is independent on pulse duration within our experimental conditions. It is reasonable by considering that our shorter limit of pulse duration is still much longer than the time constant of thermal diffusion in the conductor. In such a time scale, the transition to a normal state occurs in nearly a steady state of thermal conduction; an effective cooled perimeter becomes dominant to determine its stability. This idea is valid only in the conductor at a relatively low load factor such as our conductor.

We conclude that our conductor KISO-32 has an anisotropy in its stability margin. In the next section, the observed anisotropy in its stability margin will be investigated by another approach.

3-3-2. Measurement of Thermal Conduction in Conductor

In order to investigate the observed anisotropy of stability margin more precisely, we carried out measurements of temperature variation inside the conductor subjected to the heat pulse, and tried to estimate thermal conduction properties inside the conductor.

A. Experimental Setup and Procedure

Figure 3.3.3 shows a view of the sample of this experiment. The conductor is 340 mm length KISO-32. Its proportion of wet to total conductor surface is 50 %, which is the same as the sample for the performance test described so far. For the temperature measurement inside the conductor, unpackaged chips of thin film resistive temperature LakeShore Cryotronics Cernox™ was selected. It has fairly quick time response ~1.5 ms at 4.2 K and high sensitivity at low temperature region dR/dT ~ 10^3 Ω/K at 4.2 K, and thus, is the most suitable for our purpose, compared with other resistive thermometers or thermocouples for low temperature measurements. Figure 3.3.4 shows temperature dependence of its resistance with other types of thermometers [33]. Figure 3.3.5 and Table

3.3.1 shows its dimension and specifications, respectively. The temperature sensors are installed in 1.3 mm diameter holes bored in the conductor, with Apiezon N grease for enhancement of thermal contact. Figure 3.3.6 shows a typical cross section in which thermometers were installed. For applying heat pulse, polyimide insulated thin foil heater was installed in the same manner shown in Figure 3.3.1. at the following positions:

(1) Top surface, which is adjacent to the NbTi/Cu strand

(2) Side surface, which is adjacent to the sides of NbTi/Cu strand and Al stabilizer with Cu-2%Ni clad

(3) Bottom surface, which is adjacent to the Al stabilizer with Cu-2%Ni clad.

The assembled conductor sample was immersed in saturated liquid helium under atmospheric pressure. No current and magnetic field were applied during this experiment because we intended to examine only a thermal behavior of the conductor in pulse heating.

Rectangular pulses, of which duration is mainly 10 ms to 1 s, were inputted to heaters as simulated disturbances. It is the same condition as in conductor performance test mentioned in section 3-1. Heating power was also determined from the experimental conditions of past conductor performance tests. In particular, attention was paid to the dependence on direction of the heat flux; from top surface or bottom surface. All data were gathered by Macintosh with LabVIEW™, a data acquisition software. Schematic diagram of acquisition system is indicated in Figure 3.3.7.

B. Thermal Response Time

Before an evaluation of the experimental results, we will check thermal response time of each material at the heating section.

Characteristic time of heat conduction in material of thickness *d* can be written as

$$\tau_{th} = \frac{1}{\chi} \cdot \left(\frac{d}{2}\right)^2, \qquad (3.3.1)$$

where $\chi = \dfrac{\lambda}{C_v}$ is the thermometric diffusivity, λ is the thermal conductivity, and C_v is the specific heat at constant volume. Substituting physical properties at low temperature and the dimension of each material at the heating section to Equation (3.3.1), we get the thermal time constant of the each material. In our experimental system, the time constants of Cu sheath, NbTi/Cu strand, and PbSn, are microsecond order. The time constant of CuNi clad is relatively large, and that of the heater is furthermore large, but they are still order of several tens microseconds. However, the time constant of Apiezon N grease, which is a filler at thermometer installation position, and that of the thermometer itself are millisecond order; nevertheless they are shorter than our pulse duration. Summing up all those time constants, we conclude that the time constant of Apiezon N grease and that of the thermometer itself are dominant on this experiment; thermal response time of measurement is almost determined by those two parts, which belong to experimental matter, not to the conductor itself. Therefore, we can only discuss the temperature rise dependence on the heating spot, and cannot discuss those time delay.

3-3-3. Results and Discussion

Figure 3.3.8 and Figure 3.3.9 shows a typical result of temperature response of NbTi/Cu strand measured by thermometer buried in the conductor. Both of those pulse duration are 10 ms. Pulse input energy to NbTi/Cu strand side, of which result is shown in Figure 3.3.8, is 0.5 J. Pulse input energy to Al stabilizer side, of which result is shown in Figure 3.3.9, is 1.5 J. Heating energy ratio is 1:3 between those two, however, those two shows close temperature rise.

Figure 3.3.10 shows a result of a longer pulse. The pulse duration of signals is 1 s. Pulse input energy to NbTi/Cu strand side and to Al stabilizer side is 5 J and 10 J, respectively. Heating energy ratio is 1:2 between those two, however, temperature rise ratio is almost 3:2 as seen in Figure 3.3.10. Assuming physical properties are constant within this small temperature range, it suggests that same temperature rise requires energy ratio 1:3. It is consistent with the result at 10 ms pulse mentioned above and the result of conductor performance test. Stability anisotropy is verified experimentally.

The cause of stability anisotropy can be understandable as following. In our measurements, which are both of conductor performance test and thermal conduction measurement, characteristics of experimental condition are as follows:

(1) Response time of observed phenomenon, which is quenching or temperature rise, is above millisecond order. It is caused by both of the installation condition of heaters or thermometers and a relatively lower load factor at the test.

(2) Thermal diffusion property in the conductor is quite good. As seen in previous section, time constants of Cu sheath, NbTi/Cu strand, PbSn, CuNi clad are microsecond to several ten microsecond order.

We can infer from the condition (1) that cooling condition is approaching a steady state in that time scale. Also we can infer from the condition (2) that thermal diffusion in the conductor already reach a steady state within several milliseconds. Therefore stability anisotropy is probably caused by the difference of cooling condition depending on heating spot. To put it concretely, there is the 1:3 ratio in effective cooling area depending on heating spot. Figure 3.3.11 shows a schematic view of this idea.

In this chapter, stability anisotropy was demonstrated experimentally, and an explanation by thermal diffusion property was given to these phenomena. This knowledge serves to estimate MQE against point disturbances as seen above. Stability Margin against distributed disturbances will be discussed in the next section.

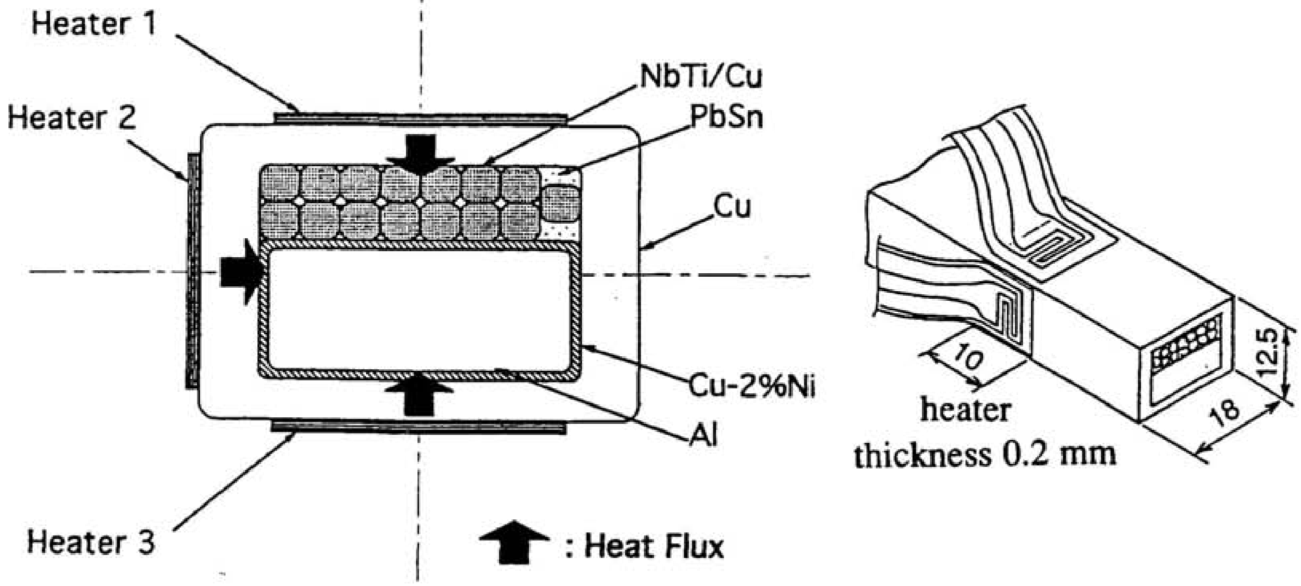

Figure 3.3.1 Schematic drawing of the arrangement of three heaters attached to the top surface, one side, and the bottom of the conductor to investigate the effect of anisotropy on the stability margin.

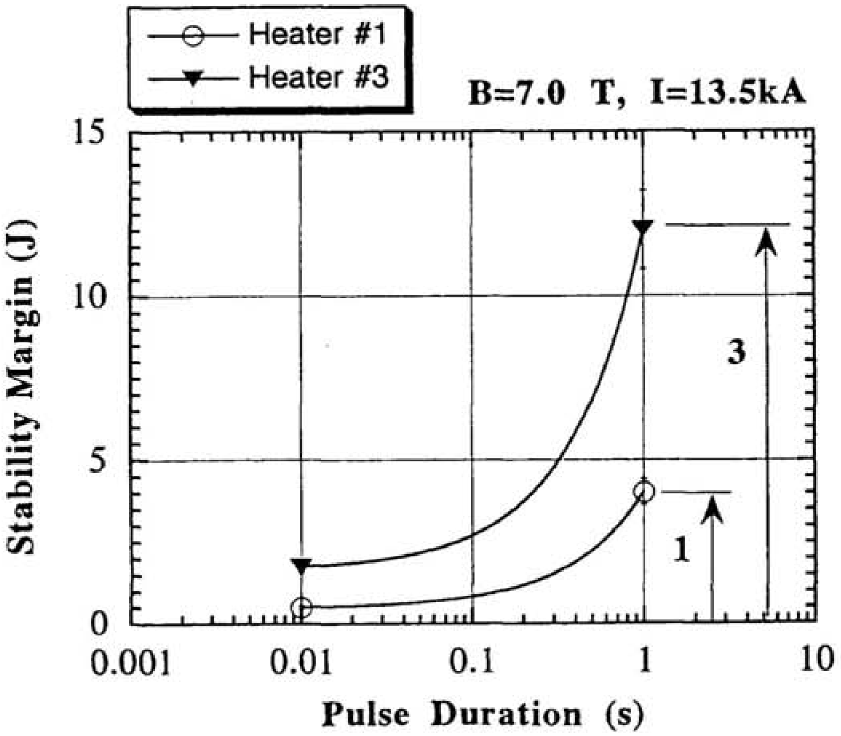

Figure 3.3.2 Dependence of stability margin on pulse duration when the direction of external heat flux is changed. Stability margin against heat flux in direction #1 is one third of that in direction #3 regardless of pulse duration.

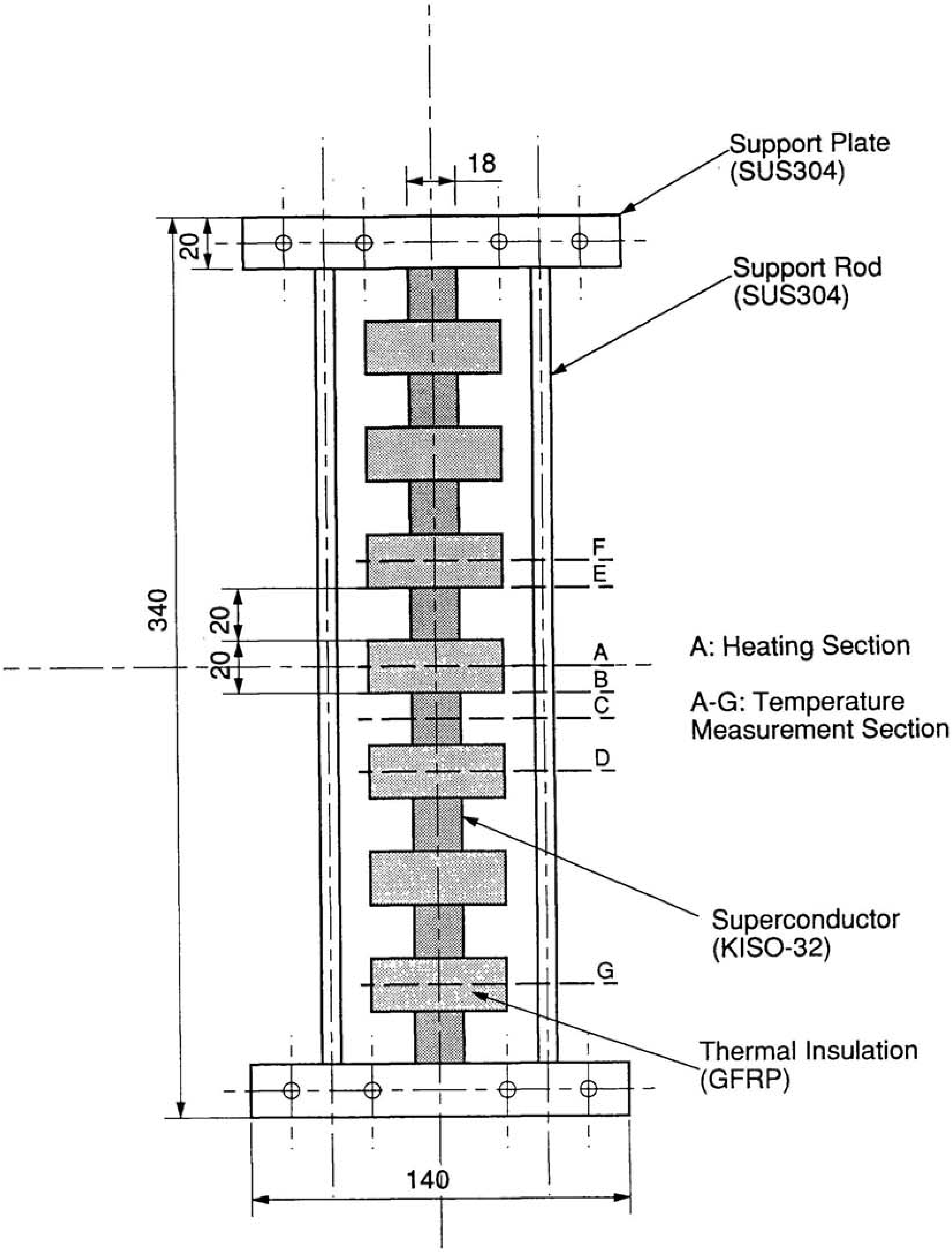

Figure 3.3.3 Conductor sample for the measurement of thermal conduction in KISO-32 conductor. Heaters and thermometers are installed beneath GFRP spacers.

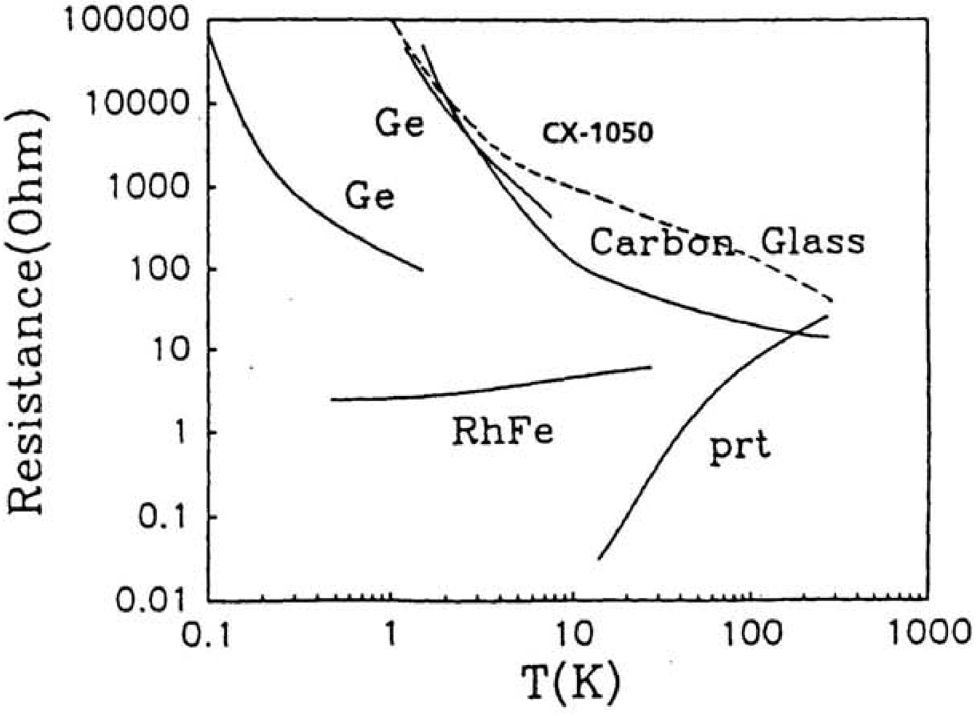

Figure 3.3.4 Temperature dependence of the resistance of typical thermometers for the cryogenic use [33]. The thermometer CX-1050, which was used in this experiment, is denoted as a dotted line.

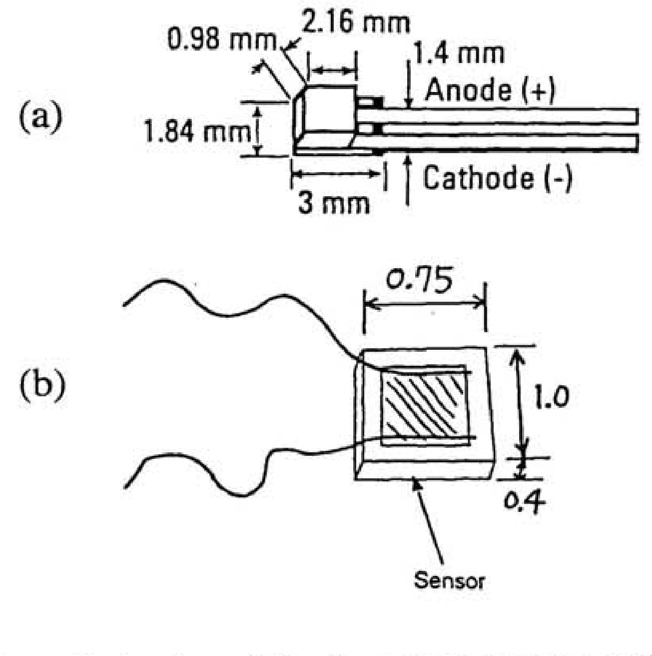

Figure 3.3.5 Schematic drawing of the thermometers used in this experiment, (a) Hermetic-cased thermometer, (b) Bare-chip thermometer. The bare-chip thermometer has quite a small size and is appropriate for installation in a limited space.

Table 3.3.1 Specification of Cernox Bare Chip thermometer

Manufacturer	LakeShore Cryotronics
Model	CX-1050 Bare Chip
Type	Thin film resistance temperature sensor
Dimension (mm)	W=0.75, L=1.0, T=0.4
Thermal response time	1.5ms at 4.2K 50ms at 77K
Useful temperature range	1K - 300K
Resistance	R~3kΩ at 4.2K R~50Ω at 100K
Sensitivity (dR/dT)	~1kΩ/K at 4.2K
Accuracy (Calibrated)	±0.025K at 1K - 100K ±0.005% at 100K - 325K
Excitation Current	~10μA
Output voltage	~30mV at 4.2K
Voltage Sensitivity (dV/dT)	~1mV / 0.1K at 4.2K

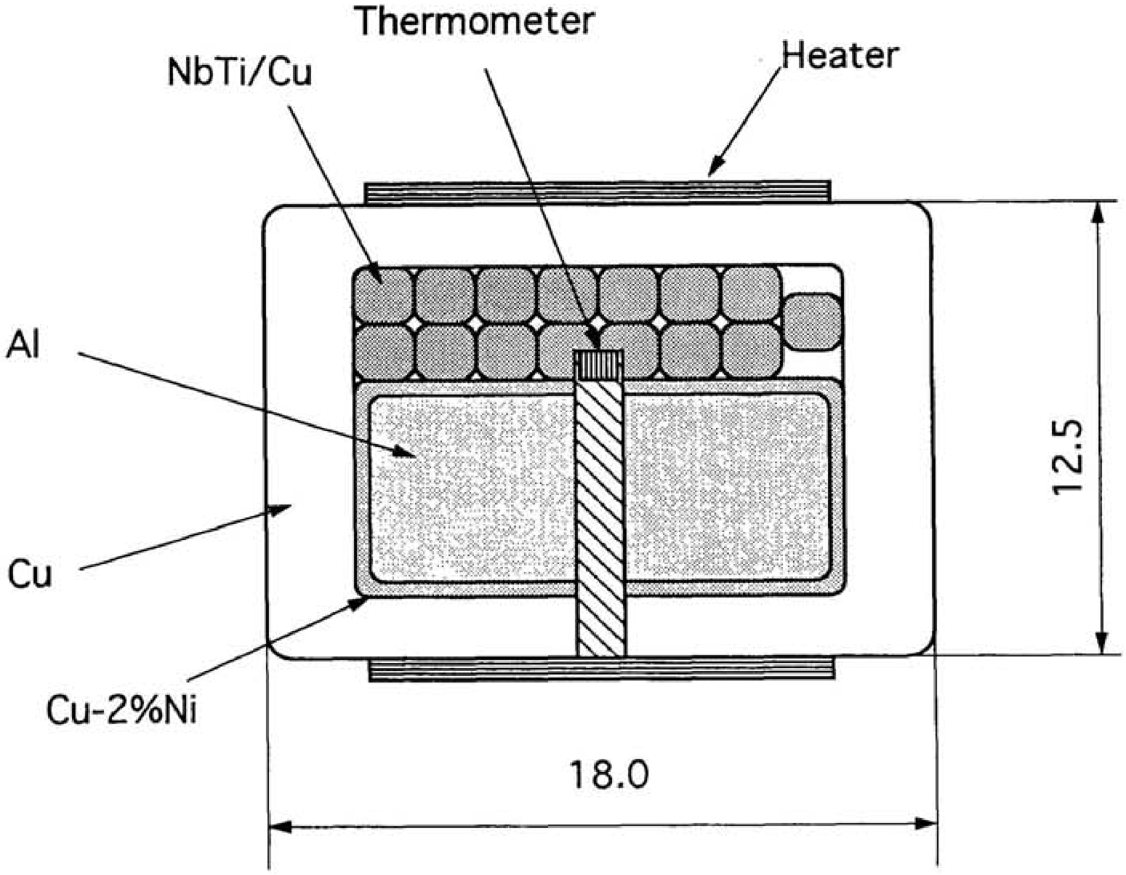

Figure 3.3.6 Typical cross section of conductor sample. A bare-chip thermometer is installed in the conductor. The hole for its installation is filled with Apiezon-N grease for good thermal contact between the thermometer and the conductor. Heaters are stuck on the top and the bottom surfaces of the conductor.

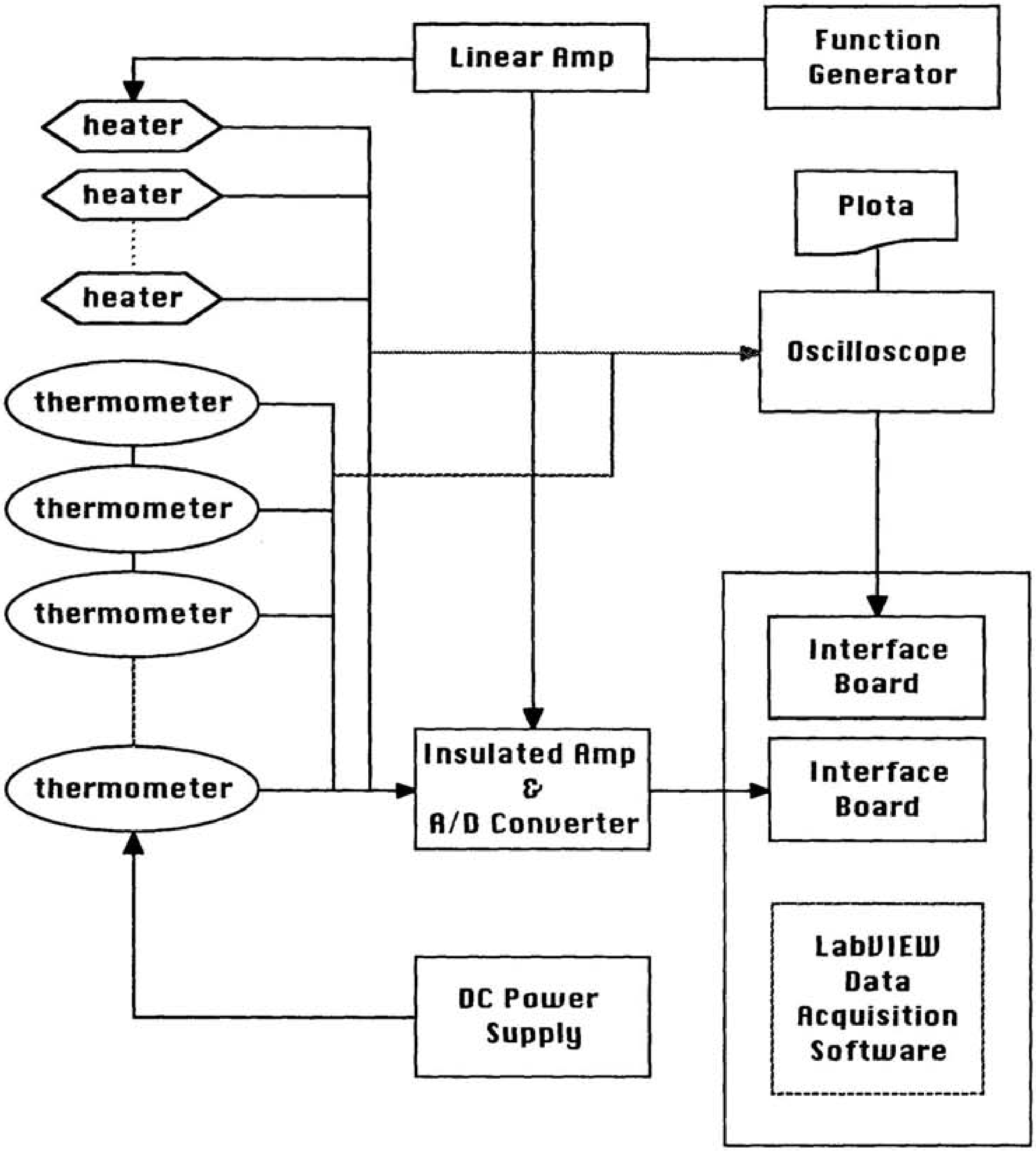

Figure 3.3.7 Diagram of the data acquisition system. All data were gathered by Macintosh™ with LabVIEW™, a data acquisition software.

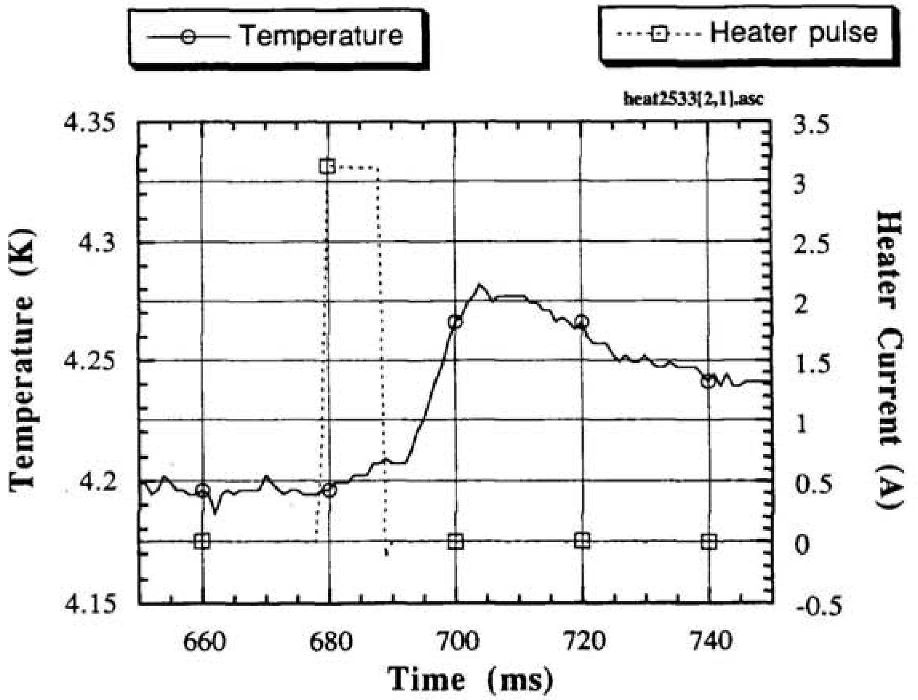

Figure 3.3.8 Time evolution of temperature of NbTi strand when the heat pulse of 10 ms - 50W is applied at the top surface adjacent to NbTi strand.

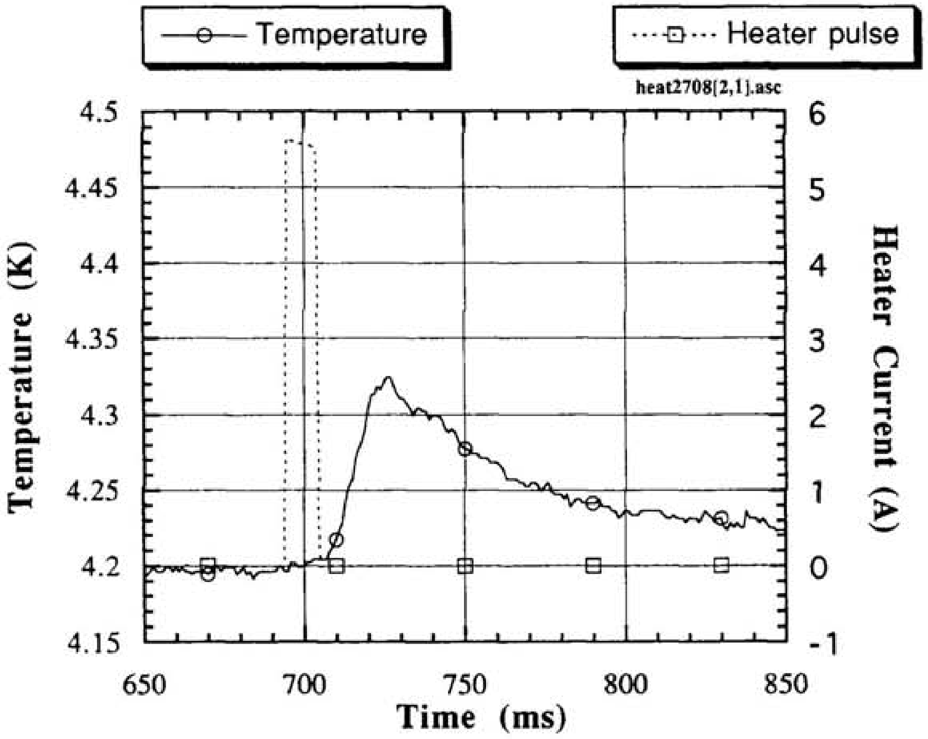

Figure 3.3.9 Time evolution of temperature of NbTi strand when the heat pulse, of which energy is three times larger than that in the case of Figure 3.3.8 ,10 ms - 150 W is applied at the bottom surface adjacent to Al stabilizer.

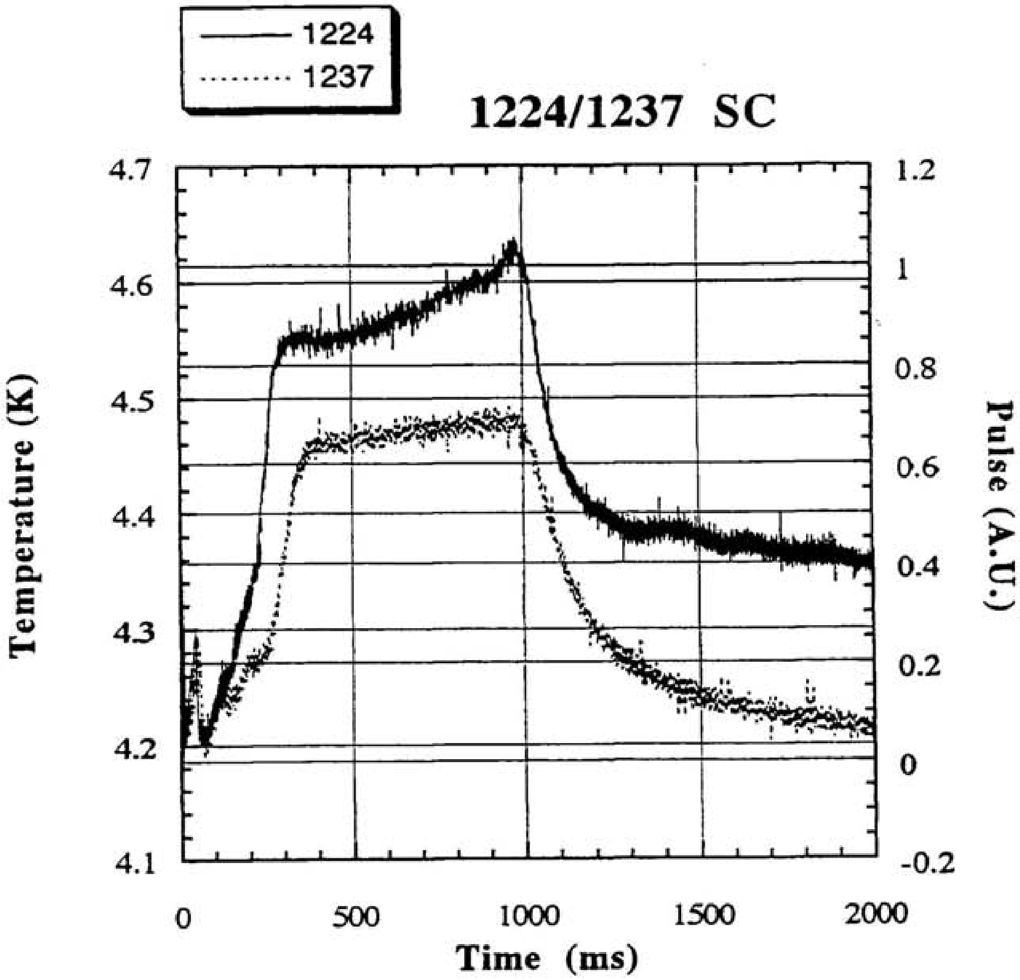

Figure 3.3.10 Time evolution of temperature of NbTi strand for longer pulse (~1 s) of 5W at top surface (1224) and 10W at bottom surface (1237). Heating energy ratio is 1:2 between those two, however, temperature rise ratio is almost 3:2. Assuming physical properties are constant within this small temperature range, it suggests that the same temperature rise requires the energy ratio 1:3.

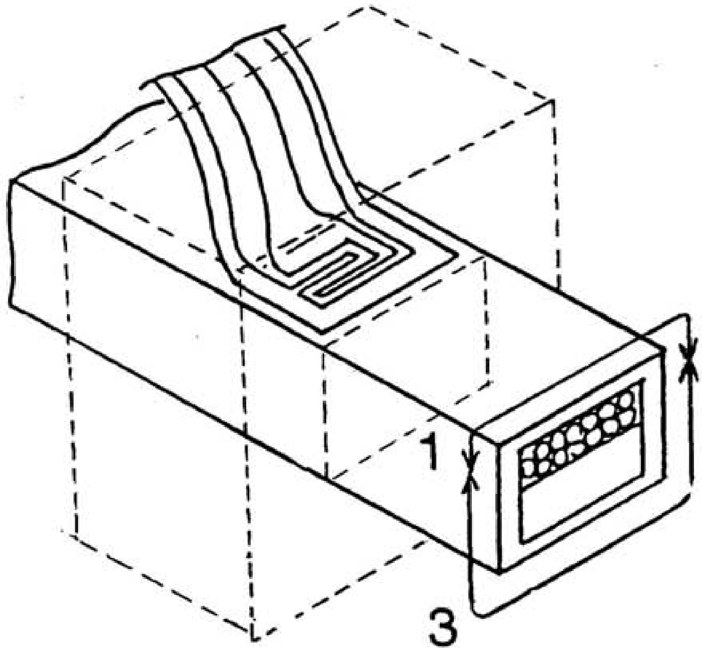

Figure 3.3.11 Schematic drawing of cooling conditions around the conductor. Anisotropy in its stability is probably caused by the difference of the effective cooling area for NbTi strand between the heat flux from the top surface and the heat flux from the bottom surface. This anisotropy is about 1:3 in energy ratio.

3-4. MQE under Distributed Disturbances

Stability margin against point disturbance was discussed in the previous sections. Disturbances are, however, probably more or less distributed in real magnets, because the main origin of the disturbance is an electromagnetic force, which should move rigid conductors in some length at the same time, not in a specific point. Pool-cooled superconducting magnets shown in Figure 2.2.2 has insulating spacers at regular pitch along the conductor, thus finite length movement of the conductor by electromagnetic force causes plural separated disturbances by friction at insulating spacers at the same time.

This type of disturbance does not agree with a usual definition of distributed disturbances by Wilson [17] in a viewpoint of its continuity along the conductor. Then, it is worthwhile to discuss this possible type of disturbance, which is a group of separated point disturbances in real magnets. In this section, experimental study and discussion about the distributed disturbances will be given.

3-4-1. Experimental Procedure

In order to investigate the stability against distributed disturbances, we planned the experiment on that subject in the conductor performance test. We installed several heaters along the conductor to simulate distributed disturbances. The heaters, which were the same type as that mentioned in section 3-3-2, were installed beneath insulation spacers in the same manner as described in section 3-1-1. Measuring method was the same as the method for the point disturbance mentioned in section 3-1-2. Figure 3.4.1 shows a schematic diagram of pulse heating in this experiment. Experimental parameters were operating current of the conductor sample, bias magnetic field, heating power, and pulse duration. They were decided with taking it into consideration that different numbers of heating spots might cause the transition to a normal state in a same operating current and a bias magnetic field, within a capacity of equipment.

3-4-2. Results and Discussion

Total input energy at which the transition to a normal state caused by heat pulse were plotted in Figure 3.4.2. We can find that the input energy increased with increasing the number of heating spots. This might be due to increase in effective cooling channel in whole heated area. The ratio of the energy was constant at 1:2:3 without depending on pulse duration when the number of heating spots is changed 1:3:5. This ratio corresponds to that of total number of cooling channels adjacent to heating spot (n+1). From the results, we can say that in order to increase stability margin, it is better to divide the energy to many points for same total disturbance energy.

On the other hand, the minimum energy density per heating spots to cause the transition to normal state, MQE_{dis}, decreased with increasing the number of the spots. The dependence can be estimated from the experimental results as following

$$\mathrm{MQE}_{point} : \mathrm{MQE}_{dis} = 1 : \frac{n+1}{2n}\ , \tag{3.4.1}$$

where MQE_{point} is the minimum quench energy against point disturbance and n is the number of heating spots. When the n is sufficiently large, MQE_{dis} converges as following,

$$\lim_{n\to\infty} \mathrm{MQE}_{dis} = \frac{1}{2} \cdot \mathrm{MQE}_{point}\ . \tag{3.4.2}$$

The decrease of the MQE_{dis} seems to be natural because the heating of its next spot prevents the spot from cooling by heat conduction along the conductor. The origin of coefficient 1/2 will be explained by the following model. Assuming the characteristic length l_{th} of temperature variation along the conductor, and the exposed length l_{ex} of the conductor per one cooling channel, the relation between l_{th} and l_{ex} determines the relation between MQE_{dis} and MQE_{point} . Case (1) ; when $l_{th} << l_{ex}$: $\mathrm{MQE}_{dis} = \mathrm{MQE}_{point}$, because one cooling channel is large enough to remove the heat energy from two adjacent heating spots. Since the cooling effect is very large, each heating spot can be considered to be completely independent on each other. Case (2) ; when $l_{th} \sim l_{ex}$: $\mathrm{MQE}_{dis} = (1/2)\cdot\mathrm{MQE}_{point}$, because one cooling channel has comparable size to remove the heat energy from one heating spots. The experimental condition corresponds to this region; temperature rise from bath temperature to T_{cs} at one heating spot is effectively cooled by one cooling channel. Case (3) ; when $l_{th} >> l_{ex}$: $\mathrm{MQE}_{dis} \sim (1/n)\cdot\mathrm{MQE}_{point}$, because one cooling channel does not have the size large enough to remove the heat energy from even one heating spot. Since the cooling effect is small, the heating effect accumulates according to the number of heating spots.

These results can be used to predict a minimum quench energy when distributed disturbances occur in actual magnets by using Equation (3.4.1). Equation (3.4.1) is of course valid under limited conditions as mentioned above, however, this method is applicable in many magnets by estimating the characteristic length of temperature variation of their conductors.

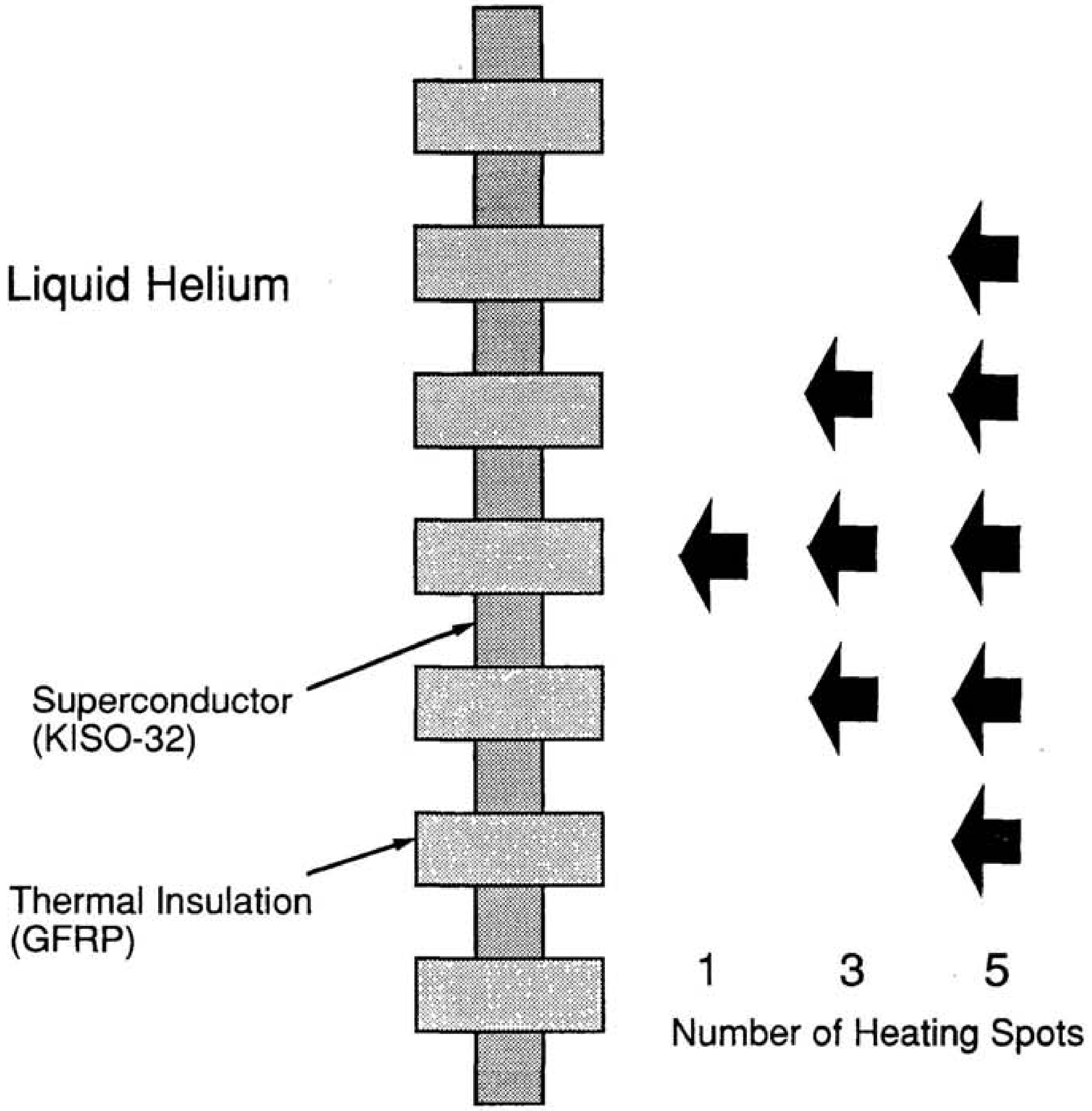

Figure 3.4.1 Concept of distributed pulse heating. Heaters are installed at one side of the conductor, beneath GFRP spacers. The number of heating spots was varied and the stability margin was investigated.

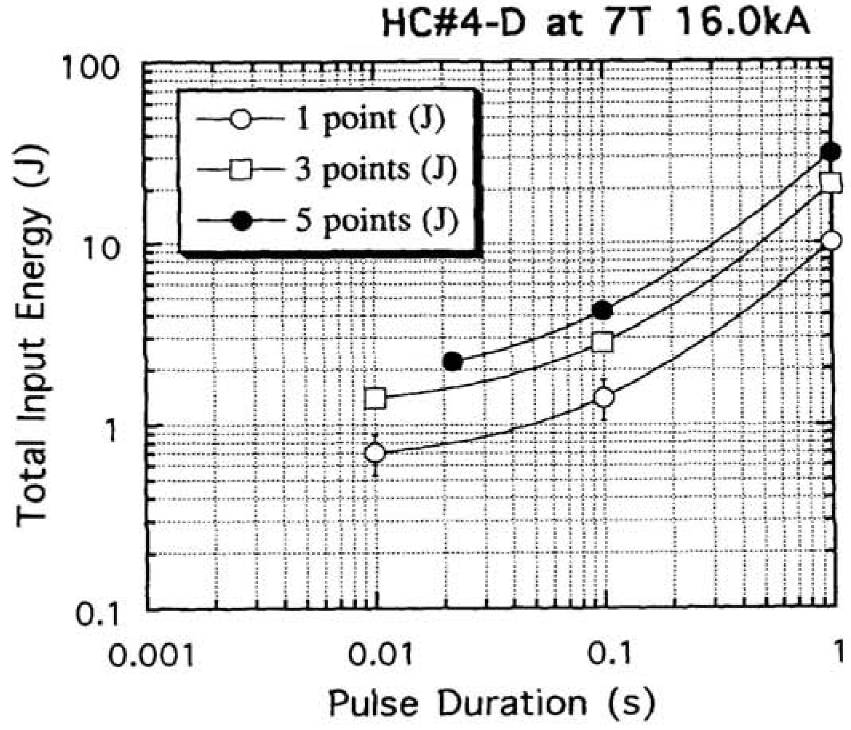

Figure 3.4.2 Total input energy to the conductor subjected to distributed disturbances of 1 point (open circles), 3 points (open squares), and 5 points (close circles). Comparison of these three cases indicates the energy ratio 1:2:3 regardless of their pulse durations.

3-5. MQE Estimation for Real Magnets

We investigated thermal behavior of a superconductor KISO-32, which is the conductor for LHD helical coils. Throughout the study of several methods to improve MQE estimation, we obtained knowledge for a MQE estimation method in real magnets. It is as follows. Each item number corresponds to section number in this chapter.

1. Stability margin experiment by simulated disturbances can give a value of experimental MQE.

2. Experimental MQE usually contains errors originated in response time of experimental setup. However, a thermal analysis can give a computed MQE value from the measured MQE value.

3. Geometrical anisotropy of a conductor probably causes an anisotropy in its stability. Experimental methods, which apply a pulse heat flux of a specific direction to the conductor, can verify an anisotropy in its stability and give a more accurate computed MQE.

4. Disturbances which distributed in longitudinal direction of the conductor give a different MQE from that against point disturbance, however the relation between MQE against point disturbance and that against distributed disturbance can be obtained experimentally by using simulated distributed disturbances.

According to this procedure, here we will show an example of MQE evaluation. In a test of an experimental conductor, which marked the recovery current of 13.7 kA at 7 T, it showed an experimental MQE of 500 mJ at 13.5 kA and 7 T. It is the value for the heat flux to strand side, i.e. this value is the smallest experimental value at the same current and magnetic field. After the evaluation of heating efficiency, which was revealed to be 10 %, its computed MQE value becomes 50 mJ. When the disturbances are distributed, the MQE value per heated spot approaches half of the value above, and total energy increases with the number of heated spots.

A. Comparison with the enthalpy of the conductor

When the duration of heat pulse approaches to zero, i.e. the energy transfer to liquid helium approaches to zero, measured MQE value should converge to minimum enthalpy of heated region of the conductor to cause quenching. Here, we calculate the enthalpy assuming that the upper limit of its temperature is current sharing temperature T_{cs}.

The current sharing temperature T_{cs} at given magnetic field and current can be obtained from equation (2.1.1) and (2.1.2) using the values of T_0=4.2 K, $T_c(0)$ =10 K and B_{c2}=10.4 T. It is estimated to be 5.31 K at B=7 T and I=13.5 kA (an experimental condition of our MQE measurements). Here we use the values of $I_c(T_0)$=1628 A from a measured critical current by its conductor manufacturer and I_C(5.31)=900 A since the number of strands are 15.

We calculate temperature dependence of the enthalpy of the conductor of 20 mm length, covered region by one insulator, as shown in Figure 3.5.1. From its fitting curve, we can see that the enthalpy change from T_0=4.2 K to T_{cs}=5.31 K is of 27 mJ. The computed MQE value 50 mJ, derived in the previous subsection, shows a fairly good agreement with this value.

B. Derivation of the permissible value of the wire movement

When we assume electromagnetic force and a friction coefficient, we can convert the computed MQE value into the permissible wire movement by the following formula.

$$\mu F x = E_{mqe} \tag{3.5.1}$$

where μ is the friction coefficient, F is the electromagnetic force, x is the wire movement, and E_{mqe} is the MQE value. The friction coefficient in low temperature has been studied by several researchers. It is ranging from 0.2 to 0.4 depending on the materials and the surface conditions [44], but we will set a typical value of the friction coefficient between copper and GFRP to be 0.3 in the following discussions.

Example 1. Electromagnetic force on a single conductor

In this case, we use the value of electromagnetic force caused by single conductor current and background magnetic field.

$$\boldsymbol{F} = \boldsymbol{I} \times \boldsymbol{B} \cdot l \tag{3.5.2}$$

where $\boldsymbol{F}$ is electromagnetic force [N], $\boldsymbol{I}$ is operation current [A], $\boldsymbol{B}$ is magnetic flux density [T], and l is conductor length [m]. Substituting I=13500 A, B=7 T, l=0.05 m yields F=4725 N. Assuming μ=0.3 and substituting E_{mqe}=50 mJ in Equation (3.5.1), we obtain x=35 μm.

Example 2. Accumulated electromagnetic force

Actually, electromagnetic force on each conductor is accumulated to some extent depending on the position of the conductor. For simplicity, we calculate this force from the maximum stress in the coil.

$$F = PS \tag{3.5.3}$$

where F is accumulated electromagnetic force, P is maximum compression stress by accumulated electromagnetic force, S is contact area between conductor and insulator. Substituting P=100 MPa [24], $S=60\times0.7\times18\times10^{-6}$ m^2 in Equation 3.5.3 yields F=75600

N, where 60 is the maximum pitch of insulators, 0.7 is the maximum covered ratio by insulators, and 18 is the longer side length of the conductor. The position, at which this accumulated force occurs, may be subjected to the different magnetic field from that in MQE measurements, but for simplicity, we use the computed MQE value described above. Assuming μ=0.3 and substituting E_{mqe}=50 mJ in Equation (3.5.3), we obtain x=2.2 μm.

The above calculation is just an order estimation of permissible wire movement. More precise calculation, however, does not take much importance, because we can not specify how conductors move in the magnet. This unknown factor makes it difficult to assume the value of the electromagnetic force and the friction coefficient. It should be noted that the value of permissible wire movement is ranging from several μm to several tens of μm. This is smaller than the attained winding accuracy of the magnet. We should energize the magnet carefully when the operating current is approaching to the rated current, which is near the recovery current.

C. *Degradation while assembling magnets*

The performance of the magnet may be lower than that of the conductor, and reasons of its degradation are described in section 1-3.

To indicate the extent of the degradation, we show an example of experimental magnets for LHD. Figure 3.5.2 shows a schematic view of an experimental magnet TOKI-MC [14], which was intended to simulate the currents and the magnetic fields of LHD helical coils. Figure 3.5.3 shows a recovery current of the magnet with that of its conductor [15]. The recovery current of the magnet at 5T and that of the conductor at 8 T are almost the same, about 14 kA. Looking at the problem from a different angle, the recovery current of the magnet is lower than that of the conductor by 15 - 20 %. There would have been several factors of this degradation, and some of them are improved in the construction of LHD, but these results suggest that we should take it into account in its operation.

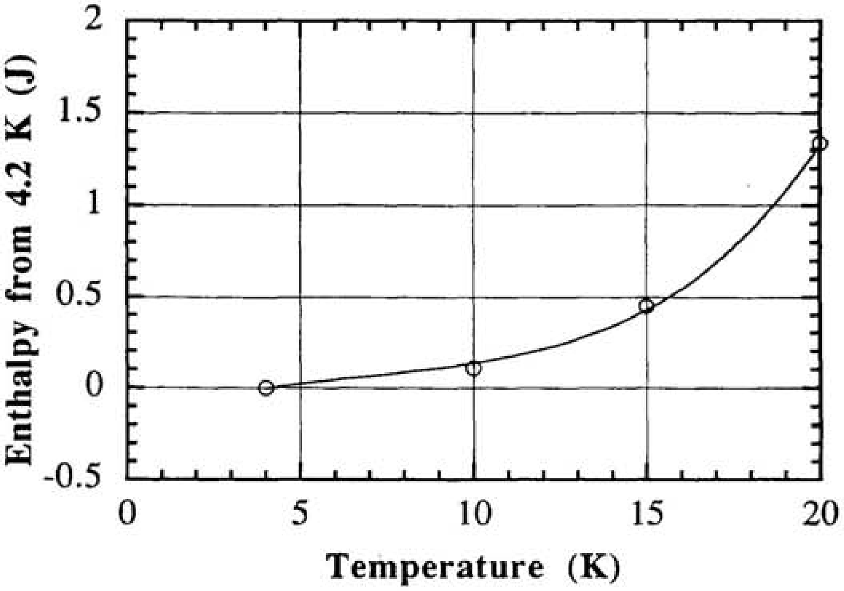

Figure 3.5.1 Enthalpy of 20 mm length KISO-32 between 4.2 K and given temperature. Open circles indicate calculated summations of specific heat of each material. A solid line shows a fitting curve from those values.

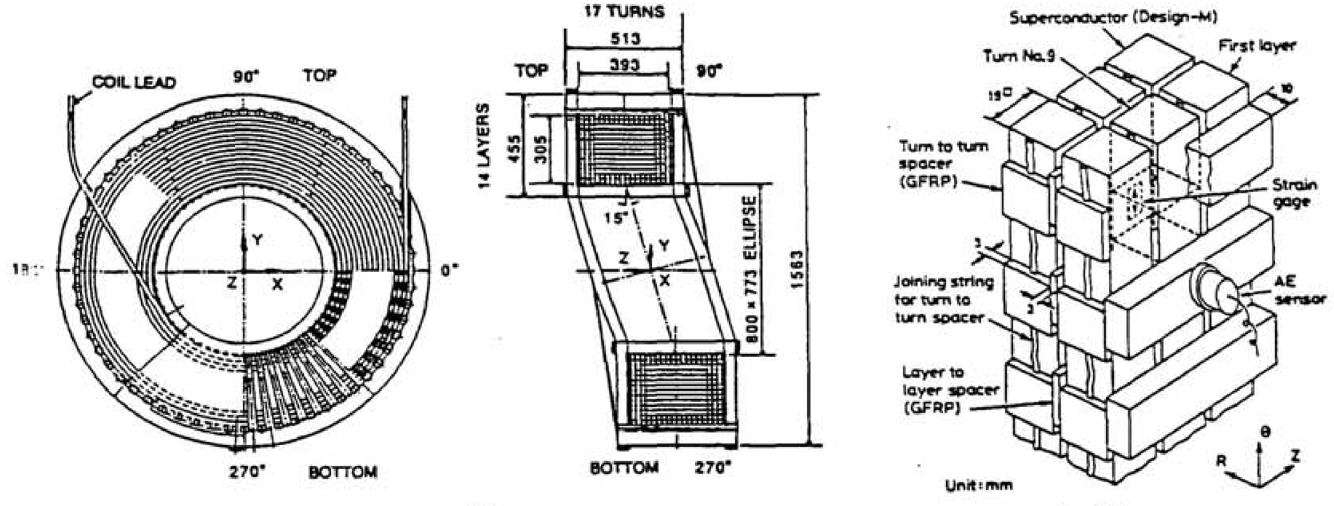

(a) (b)

Figure 3.5.2 Schematic view of an experimental magnet TOKI-MC, (a) Cross-sectional view, (b) Spacer structure [14].

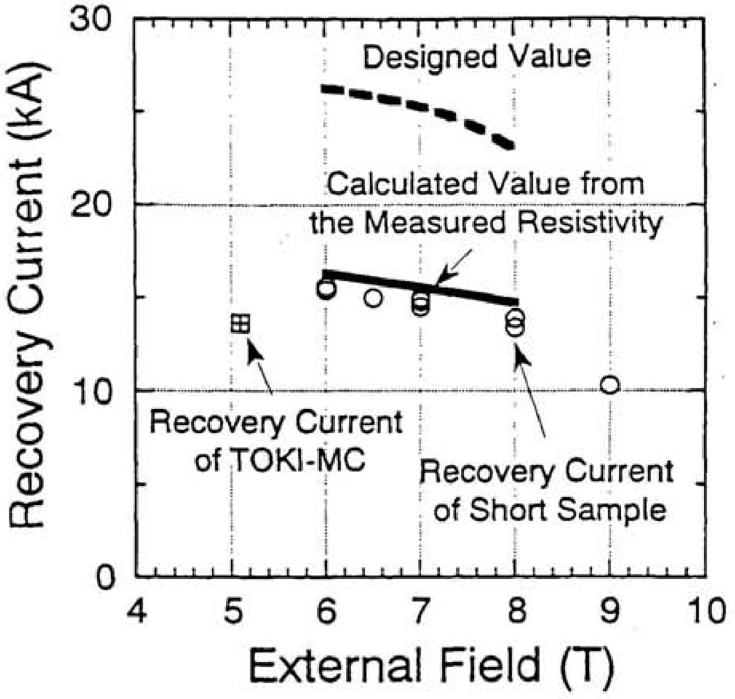

Figure 3.5.3 Recovery current of the conductor for TOKI-MC [15]. The recovery current of the magnet at 5T and that of the conductor at 8 T are almost the same, about 14 kA. Looking at the problem from a different angle, the recovery current of the magnet is lower than that of the conductor by 15 - 20 %.

4. Development of an Advanced Method for Helical Coil Winding

Superconducting helical coils require compliance with a great number of design and manufacturing specifications as described in Chapter 2. Winding accuracy, however, is the crucial factor of the manufacturing process. This chapter describes the development of an advanced method for helical coil winding.

4-1. Winding Research and Development

4-1-1. Principles of Helical Coil Winding Methods

In coil winding processes, tension winding methods have been employed so far. We first describe an example of these conventional methods, then an idea of helical coil winding.

A. Cylindrical Coils

In manufacturing cylindrical coils or D-shape coils, which are mainly used in tokamaks, tension winding methods can be used to reduce gaps between layers to increase rigidity of coils, as shown in Figure 4.1.1. Hoop stress along the conductor of cylindrical coils which are wound with constant tension may be written

$$\sigma_E(x)=\sigma_0[1-\ln\{(x_0+a)/(x+a)\}]. \qquad (4.1.1)$$

where $\sigma_E(x)$ is the hoop stress after the winding process, σ_0 is the given constant tensile stress in the winding process, x_0 is the radial thickness of the coil, a is the equivalent radial thickness of the bobbin whose elasticity is assumed to be the same as the coil's, x is the radial position of the coil. The hoop stress caused by this method works to reduce gaps between layers to increase the rigidity of coils.

There are several manners of tension variation during winding processes, including the one above. For other example, an inclined tension method, in which tension is gradually decreased as x increases in Figure 4.1.1, enables to reduce unevenness of residual tension in its radial direction. A recently developed winding method, which uses a conductor with a surface insulation of imperfectly-cured resin, utilizes another inclined tension method, in which tension is gradually increased as x increases in Figure 4.1.1. This winding method is an alternative of resin-impregnation method, thus it attach more importance to the rigidity perpendicular to the conductor than tension uniformity of all conductors.

Each method above is different in tension variation manner, however, when the tension is applied to the conductor is the same regardless of tension variation manner. The tension can be applied to the conductor during only its winding process. As an exception, there is a method which utilizes the difference between the thermal contraction property of the bobbin and the one of the conductor, however we will not discuss it here.

B. *Helical Coils*

In helical coils, the loci of coils are not two-dimensional as seen in cylindrical or D-shaped coils. We can not adopt tension winding method described in previous section, hence we need some other contrivance to achieve their winding processes.

In order to trace their loci three-dimensionally, pre-shaped helical bobbins to guide conductors has been used so far. The bobbins are used for both of plasma vacuum vessel and coil case, after the coil winding processes. The bobbins are made by the press using helical-shaped molds, or by direct numerically-controlled machining. An example of the former is the one for the Heliotron-E, an example of the latter is the one for the Compact Helical System (CHS) [34]. This winding method realize helical forming of conductors by mainly pressing conductors against the bobbins. Also auxiliary special jigs or equipment, helical guides etc., are often utilized [22].

The method above is for continuous winding of helical coils, however there are other winding methods: segmented design of helical coils or modular helical coils. An example of the former is the one for the Advanced Toroidal Facility (ATF) [5], and an example of the latter is the one for the Wendelstein VII-AS [6]. We will not mention their details here, however it should be emphasized that conductors are formed into helical-shape mainly by pressed against helical-shaped fixtures or splittable molds. It is the same concept as the one of conventional continuous winding methods mentioned above.

In recent years, the construction of more elaborate or superconducting helical coils has been proposed from a viewpoint of performance improvement as a fusion experimental device [2][35][36]. Construction of such coils requires more accurate positioning of conductors than the devices before, thus requires not only manufacturing of accurate helical bobbins, but also direct forming of conductors into helical-shape. In particular, superconducting helical coils require minimum joints, which are main origin of heat load in windings, hence continuous helical-shape forming is inevitable. In the next section, winding R&D of the LHD will be described.

4-1-2. Experimental Coils

As has been mentioned in the previous section, the winding of superconducting helical coils requires continuous conductor forming, which was not established in the constructions of former helical devices. In this section, two types of R&D coils intended for development of the manufacturing technology extrapolatable to the construction of the LHD will be described. Major items and parameters of R&D coils are listed in Table 4.1.1.

A. TOKI-WT

TOKI-WT is a sectional 110 ° winding test coil, the major dimensions of which was the same as those of the LHD [12]. The purpose of the coil was to provide engineering data on the helical shaping of the conductor and fabrication techniques for the cooling channels. A copper conductor having almost the same mechanical properties as the superconductor was used. Figure 4.1.2 and 4.1.3 show a schematic view of the TOKI-WT and a cross-sectional view of its winding, respectively.

Its conductor is 29 mm × 22 mm size half-hardened copper. Turn-to-turn insulator is 6 mm thick Glass-Fiber Reinforced Plastic (GFRP), and layer-to-layer insulator is 2 mm thick or double 1 mm thick GFRP. The main feature of its winding method is the following: pre-forming into average curvature of conductors' loci, in-situ twisting by utilizing special hydraulic jig, pressing conductors against helically arranged ties. This winding method is a partial extension of conventional helical coil winding methods. It was proved to be fare effective, however, it left problems of its curvature forming, conductor size, and three-dimensional insulator shaping. Figure 4.1.4 and 4.1.5 show a picture of TOKI-WT and a magnified view of its winding surface. In Figure 4.1.5, we can see the inclination of each conductor to a same direction at the bottom of the torus. It is inferred that only an average curvature forming, which is for only the direction of conductor's height, is not sufficient for the winding of such large sized conductor.

B. TOKI-HB

TOKI-HB was designed and fabricated to demonstrate the feasibility of constructing a pool-cooled superconducting helical coil [37]. One of the most important purposes of this R&D work is to establish a coil winding technique as well as superconducting magnet technology [38]. Figure 4.1.6 shows a schematic view of the TOKI-HB. Its major parameters are listed in Table 4.1.2. The major radius of its helical coil is 0.8 m, about one-fifth of that of the LHD, which is considered to be large enough to be extrapolatable to the LHD. In the following, only its winding processes are described.

The locus of the conductor is helical along the hollow torus and is not a geodesic line. This characteristic of its locus is the same with the LHD. Thus, the conductor cannot be wound with tension, and it is necessary for the winding, which forms the conductor, to utilize plastic working in three dimensions: in-plane curvature, out-of-plane curvature, and torsion. Furthermore, because the degrees of those three workings depend on a spatial point along the locus, the conductor forming must be numerically controlled. Therefore, a special winding machine was designed.

Figure 4.1.7 shows the coil winding machine. The forming head of the winding machine can form the conductor into arbitrary shape along its locus. The maximum value of the in-plane curvature, the out-of plane curvature and the torsion is 2.07×10^{-3} mm^{-1}, 1.83×10^{-3} mm^{-1}, 4.10×10^{-3} $\mathrm{rad{\cdot}mm}^{-1}$, respectively. The winding was done continuously by toroidal rotation of the hollow torus and poloidal rotation of the forming head. The forming head has several degrees of freedom to avoid interference with the transitional locus of the conductor during winding.

Figure 4.1.8 shows the special "shovel gauge" for measurement of the winding. The spatial position of the conductor in the minor radial and transverse direction was measured by the gauge setting in the perpendicular plane of the tangential vector on the locus. Coil winding was done with a measurement of the whole conductor at the end of the winding of each layer. The total number of measurement points is more than 3000. As a result, we achieved an accuracy of less than 1.5 mm in both the radial and transverse direction.

After its completion, TOKI-HB successfully achieved its rated current 8.93 kA under the fully stabilized criterion [39].

4-1-3 Results and Discussion

Previous two types of R&D coils gave the following engineering information on winding technique.

In TOKI-WT, the lack of in-plane curvature forming caused the inclination of each conductor to a same direction at the bottom and the top of the torus. Helical coil winding with cooling channel absolutely requires in-plane curvature forming, even if its value is much smaller than that of out-of-plane curvature. In addition, the size of the conductor should be as small as possible from the viewpoint of the conductor forming.

TOKI-HB demonstrated the validity of those technical conditions which was posed by TOKI-WT, and furthermore, it also demonstrated the effectiveness of the winding machine which realize continuous three-dimensional forming. However, both of these R&D coils left problems that originated from its inherent non-tension winding. It is the augmentation of coil height especially at the bottom of the torus. It is due to the self weight of its winding, and has been always a serious problem in helical coil winding so far.

We have to solve this problem to realize the helical coils of the LHD. The method which can prevent the augmentation of coil height will be described in the next section.

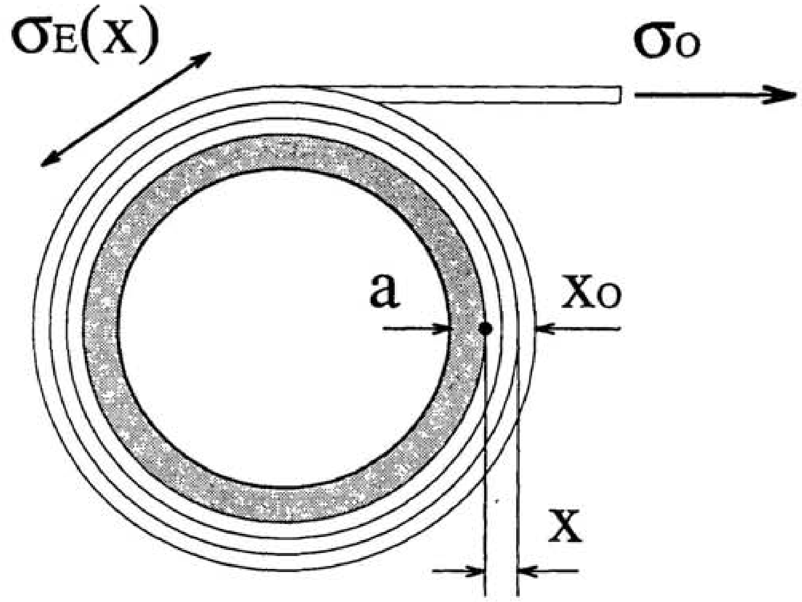

Figure 4.1.1 Conventional tension winding method for cylindrical coils. $\sigma_E(x)$ is the hoop stress after the winding process, σ_0 is the given constant tensile stress after the winding process, x_0 is the radial thickness of the coil, a is the equivalent radial thickness of the bobbin whose elasticity is assumed to be the same as that of the coil, and x is the radial position of the coil. The hoop stress caused by this method works to reduce gaps between layers to increase the rigidity of the coils.

Table 4.1.1 Winding Specifications of R&D Coils with LHD

Device Name	LHD	TOKI-WT (R&D)	TOKI-HB (R&D)
R&D Objective	---	Demonstration of Large-Size Helical Winding with Cooling Channels	Demonstration of Superconducting Helical Coil System
Major Radius	3.9 m	4.0 m	0.8 m
Minor Radius	0.975 m	0.96 m	0.2 m
Toroidal Period Number	10	5	3
Poloidal Period Number	2	1	1
Pitch Modulation Parameter	0.1	0	0
Material of Conductor	NbTi Composite Superconductor	Half-Hardened Copper	NbTi Composite Superconductor
Conductor Size	12.5 x 18.0 mm	29.0 x 22.0 mm	8.0 x 16.0 mm
Number of Turns	450	33	112
Target Winding Accuracy	5 x 1E-4	---	1.0 x 1E-3

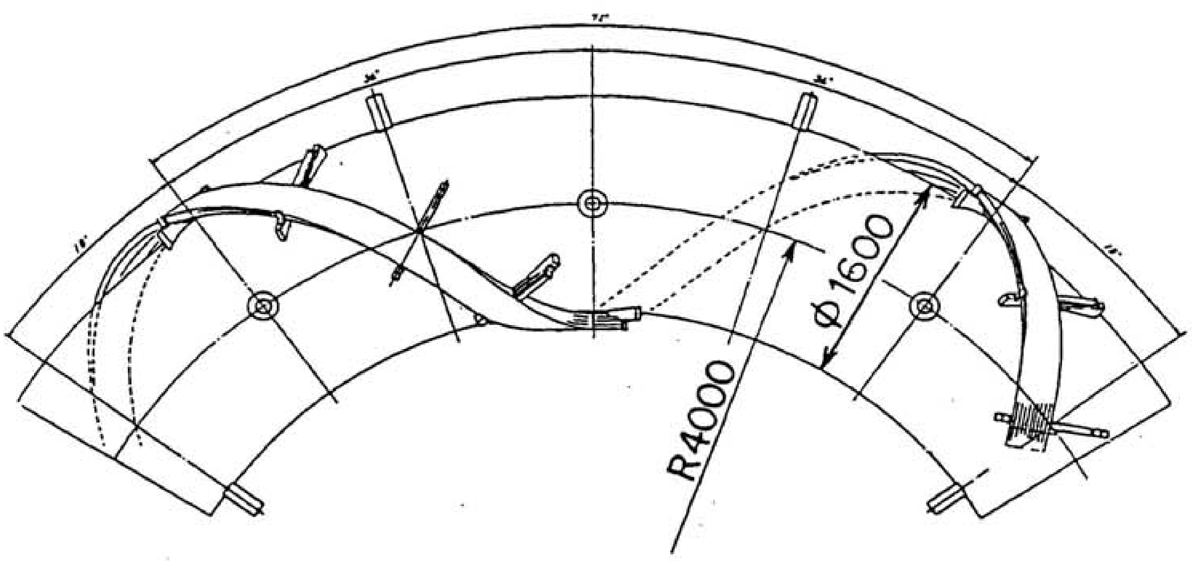

Figure 4.1.2 Schematic view of partial winding R&D coil TOKI-WT. The purpose of the R&D was to provide engineering data on the helical shaping of the conductor and fabrication techniques for the cooling channels. It consists of an iron-made partial torus, occupying a 110° section of the complete torus, and a model helical coil made of copper conductors. The major dimensions of this R&D were almost the same as those of LHD.

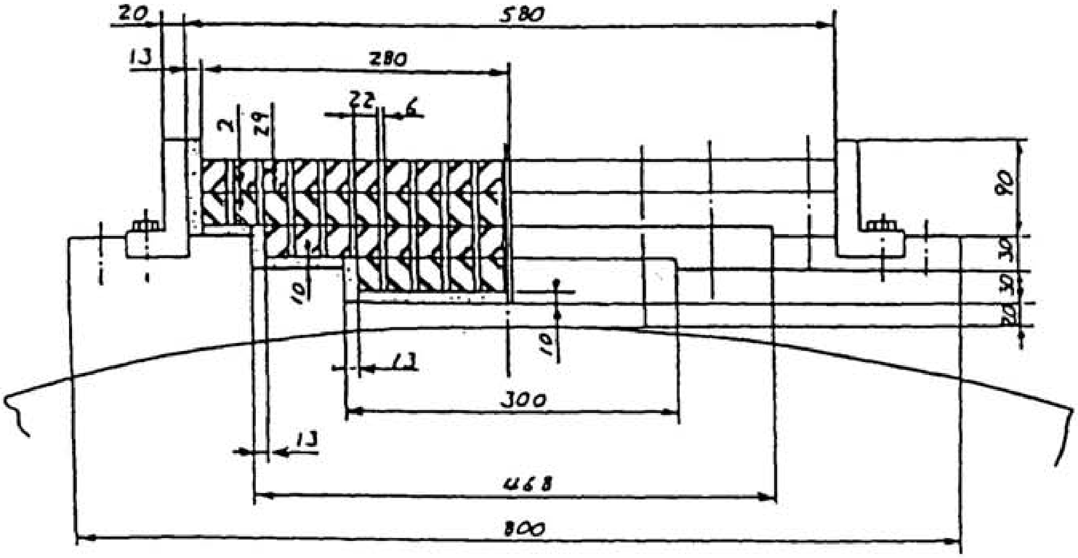

Figure 4.1.3 Cross-sectional view of TOKI-WT coil winding. Its conductor is 29 mm × 22 mm size half-hardened copper. Turn-to-turn insulator is 6 mm thick Glass-Fiber Reinforced Plastic (GFRP), and layer-to-layer insulator is 2 mm thick or double 1 mm thick GFRP.

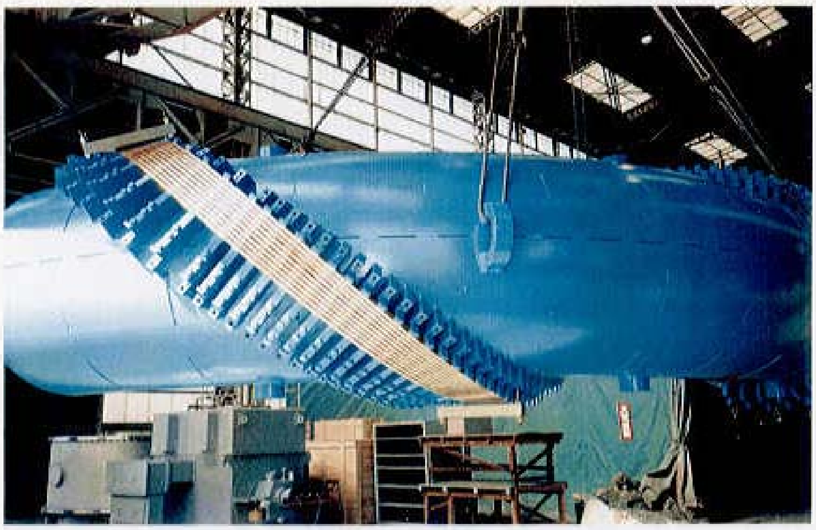

Figure 4.1.4 Picture of the completed TOKI-WT. The model helical coil was wound on the ties arranged helically on the torus; the conductors were pre-formed into average curvature of their loci, twisted in-situ by utilizing special hydraulic jig, and pressed against the ties.

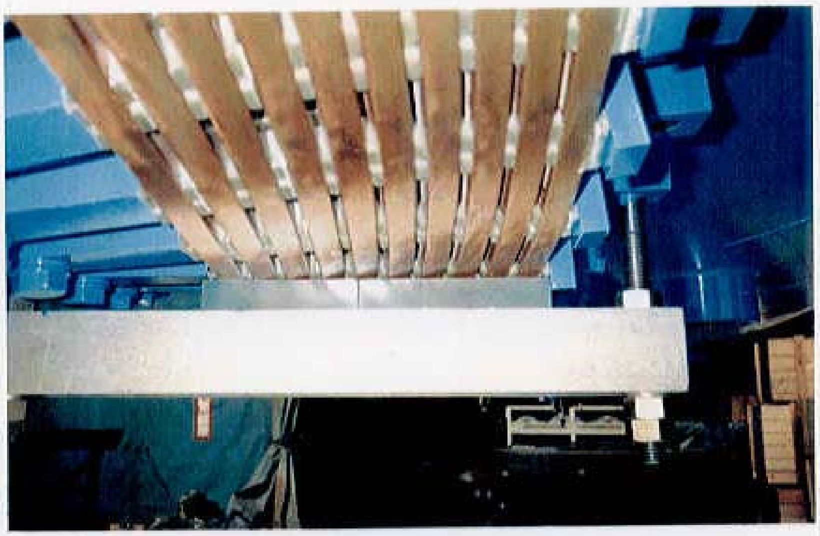

Figure 4.1.5 Magnified view of the winding surface of TOKI-WT. Each conductor inclines to the same direction, which is the radial direction of the in-plane curvature. This result suggests that only an average curvature forming, which is for only the direction of conductor's height, is not sufficient for the winding of such a large sized conductor.

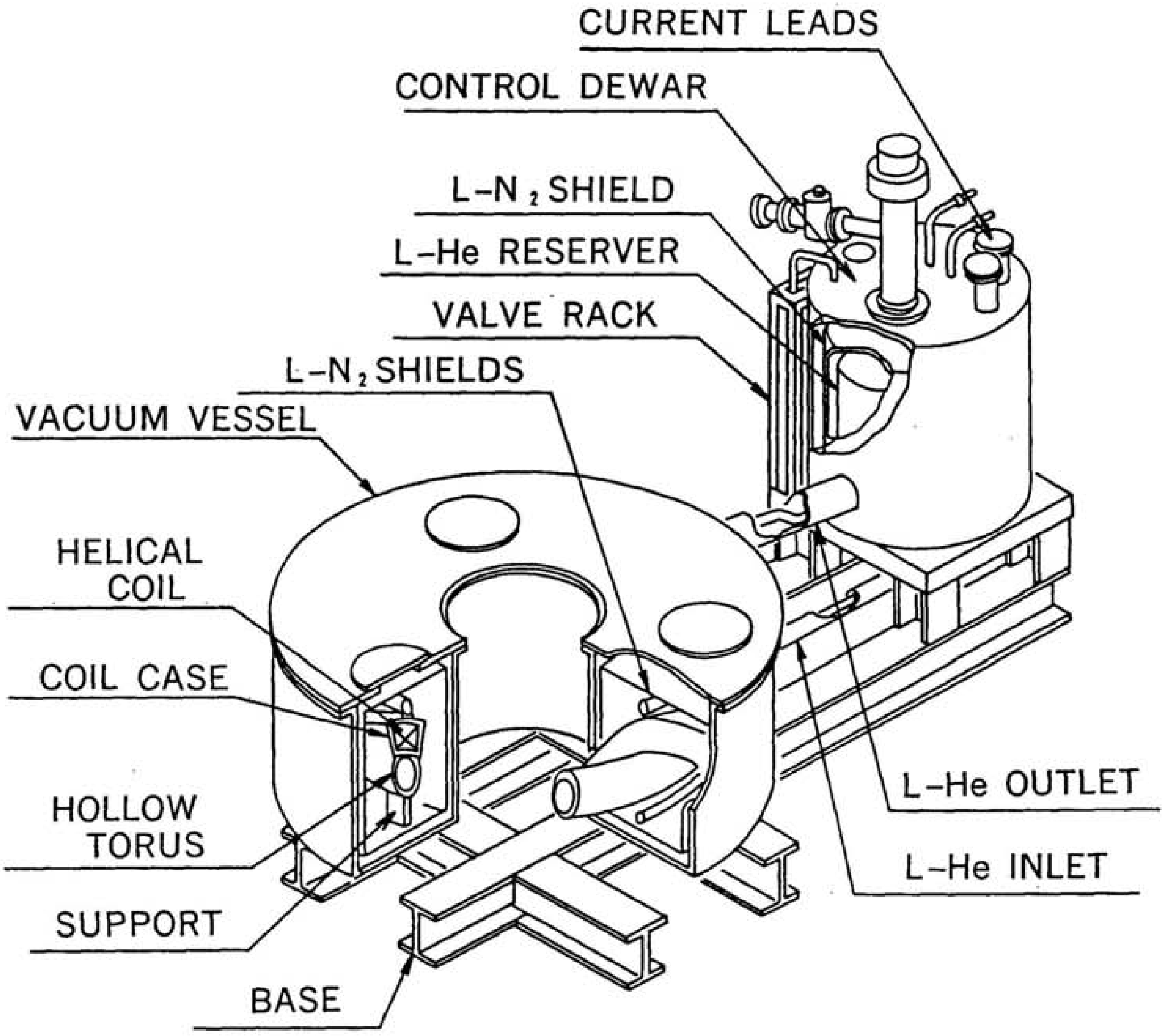

Figure 4.1.6 Schematic view of the superconducting helical R&D coil TOKI-HB. This device was designed and fabricated to demonstrate the feasibility of constructing a pool-cooled superconducting helical coil. One of the most important purposes of this R&D work was to establish a coil winding technique as well as superconducting magnet technology. The major dimensions were about one-fifth of that of the LHD. After completion, its rated current 8.93 kA was successfully achieved under the fully stabilized criterion.

Table 4.1.2 Major parameters of the superconducting helical R&D coil TOKI-HB.

Item	Parameters
Major radius (m)	0.8
Minor radius (m)	0.2
Winding rule	$l = 1$, $m = 3$
Magnetomotive force (MA)	1
Operating current (A)	8930
Number of turns	112
Inductance (H)	0.048
Stored energy (MJ)	1.9
Maximum field (center) (T)	0.75
Maximum field (coil) (T)	3
Stability parameter	0.6

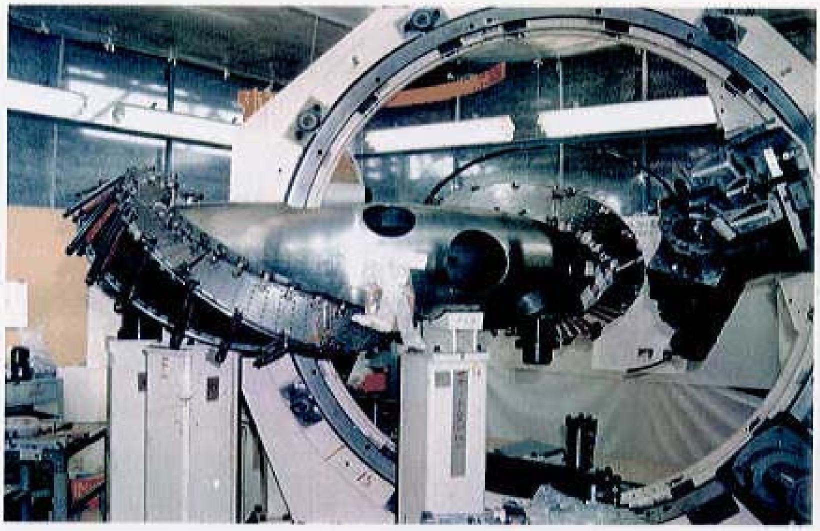

Figure 4.1.7 Coil winding machine for TOKI-HB. This machine was numerically controlled in accordance with the helical loci of the conductors. The winding was done continuously by toroidal rotation of the hollow torus and poloidal rotation of the forming head. The forming head of the winding machine formed the conductors into arbitrary shapes along their loci.

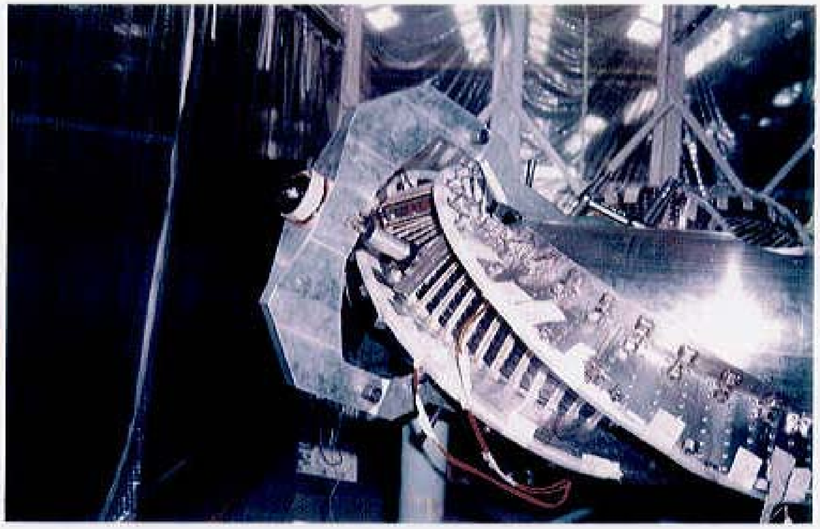

Figure 4.1.8 Measurements with special "shovel gauge". The spatial positions of the conductors in the minor radial and transverse directions were measured by the gauge setting in the perpendicular plane of the tangential vector on the locus. The measurements of the conductors were done at each completion of layers. The total number of measurement points was more than 3000.

4-2. Proposal for Acquired Tension Winding

4-2-1. Theory of Tension Acquisition

A. *Geometrical Characteristics of LHD Helical Coils*

In helical coil winding, it is necessary to wind conductors in accordance with its locus equation. The overview and cross section of the LHD helical coil and the cross section of the conductor are shown in Figure 4.2.1. The locus of the helical coil has in-plane curvature, out-of-plane curvature, and torsion as shown in Figure 4.2.2. Each conductor has its own locus which has its own profile of curvatures and torsion. A typical profile of locus is shown in Figure 4.2.3, which shows curvatures and torsion vary as poloidal angle. Especially the in-plane curvature positive-negative sign changes at every poloidal 180 degrees. Other nonplanar coils in helical devices are similarly situated, thus this feature made it necessary to utilize accurate molds or winding guides so far [6][22]. In recent years the demand for constructing more elaborate or superconducting nonplanar coils makes it necessary to utilize three dimensional plastic working of the conductor in the coil winding process [38][40][41]. However, it is often insufficient to achieve the required winding accuracy.

B. *Concept of Acquired Tension Winding Method*

In the winding process of helical coils, external direct tension causes a shift of discrepancy perpendicular to the conductor axis because the locus of the conductor is not a geodetic line. Thus external tension works to reduce the conductor's own tension in the end. In addition, external tension deforms the conductor's own shape which is given by a forming head before coil winding. We developed a new complementary winding method that enables us to produce acquired tension along the conductors. The method is; after winding each layer, the layer is pushed to shift perpendicularly to the conductor axis, from the shorter path's side to the longer path's side, utilizing its in-plane curvature. This is shown in Figure 4.2.4 as a development drawing along a helical coil.

This shift works to reduce the gap under the conductor and produce tension along the conductor. The relation between shifted value and displacement in the direction of minor radius can be described with the simplified model which assumed the locus of the helical coil to be an arc which has a constant in-plane curvature and a constant out-of-plane curvature [42]. It is shown as follows:

$$\Delta w_R=\rho_F/\rho_E\ \Delta h_R \qquad (4.2.1)$$

where Δw_R is the shifted value for Δh_R, Δh_R is the displacement in the direction of minor radius, ρ_F is the out-of-plane curvature, ρ_E is the in-plane curvature.

Residual tensile stress be this method may be written

$$\sigma=\varepsilon_T E \qquad (4.2.2)$$

$$\varepsilon_T=\rho_E \Delta w_T \qquad (4.2.3)$$

$$\Delta w_T=\Delta w_A - \Delta w_R \qquad (4.2.4)$$

where σ is tensile stress, ε_T is tensile strain, E is modulus of elasticity, Δw_T is shifted value converted into residual tension, Δw_A is actual shifted value.

Formulas (4.2.1) - (4.2.4) result in residual tensile stress at each layer in the winding process. Here it is not considered the effect of stress relaxation by accumulation of layers as shown in formula (4.1.1). The tensile stress is expected to improve rigidity of the coil.

4-2-2. Real-Scale Winding Trial

We applied this winding method to a real-scale helical coil winding trial of the LHD [21], which was carried out in Hitachi works before in situ winding. The real-scale winding trial was planned and carried out on the basis of past R&D: TOKI-WT, TOKI-HB, several winding machine R&D, material R&D for the coil, and manufacturing technology R&D. Its chief objectives are as follows:

(1)To test-run and adjust the winding machine.

(2)To decide shapes and configurations of elements of the helical coil.

(3)To develop various winding methods and to optimize them.

(4)To develop systems of measuring spatial positions of the helical coil.

(5)To get used to real winding surroundings.

We describe mainly the third objective in this list, in particular, the acquired tension winding method.

A. Configuration of the R&D Test Coil

Figure 4.2.5 shows the winding machine and the test coil for the winding trial. Major parameters of this winding trial are listed in Table 4.2.1 with those of the LHD. The R&D test coil is its real scale of the LHD ; its major radius is 3.9m, minor radius is 0.975m, however, the number of turns is 22 compared with 450 for LHD. The test coil is a mock-up pool-cooled superconducting coil which was assembled from a coil can model, composite superconductors and insulation spacers. The conductor was the same one for LHD, shown in Figure 4.2.1. It was formed into a helical shape by the forming head in the winding process. Insulation spacers were made of newly developed GFRP which was characterized by low thermal contraction and high mechanical strength. They were also given torsion and curvatures in advance. The coil can was made of iron and stainless steel machined by numerical control. The inner surface of the stainless steel coil can was covered with a newly developed autoclave-insulation which was superior to conventional hand-lay-up insulations in low thermal contraction and high mechanical strength.

B. Winding Process

We first build the conductors three-dimensionally with the winding machine which had specially been developed. After fabricating each layer, we applied the method mentioned above. Finally, the displacement and the strain which each conductor produced was measured. The variation of residual gaps between the bottom surface of the conductors and layer-to-layer insulators was measured as the displacement of the top surface of the conductors by digital slide calipers. The number of measured points was over 10,000. Maximum shifted value for the acquired tension was 5mm. The residual tension of the conductor was measured by two axis strain gauges attached to the surface of the conductors.

4-2-3. Results and Discussion

A. Variations of the Gaps

Several cases of pushed value were tried, three typical cases are shown in Figure 4.2.6.

Its horizontal axis shows cases of pushing conductors, its vertical axis shows measured displacement of conductor surface levels. Case(a) indicates non-shifted layer, case(b) indicates layer which was pushed in the whole range with a uniform displacement and case(c) indicates layer which was pushed with gradually changed values along the conductor following the sine curve.

Cases(b) and (c) clearly show an effect of the new method; the measured levels of conductors' surface are lower than in case(a). In addition, case(b) is superior to case(c) in respect of reduced level. When the Δw_A in the trial was 5 mm, which was the actual value, its reducible level was 2 mm with representative curvatures ρ_F: 6.25×10^{-4} mm^{-1} and ρ_E: 2.5×10^{-4} mm^{-1}. This 2mm is several times larger than gaps in the actual winding process, thus the Δw_A: 5 mm is large enough to improve the quality of the winding. The actual reduced level Δh_R at case(b) was about 0.3 mm, the difference between those: 1.7 mm is a margin to leave tension along the conductor.

B. The Residual Tension

The residual tensile stress along the conductors can be estimated by formulas (4.2.1) - (4.2.4). A trial calculation for σ yields 105 MPa with Δh_R=0.3 mm, ρ_F =6.25×10^{-4} mm^{-1}, ρ_E =2.5×10^{-4} mm^{-1}, Δw_A=5 mm, E=99 GPa. Figure 4.2.7 shows the longitudinal tensile stress along the conductors converted from measured strain. Its horizontal axis shows the longitudinal position along the conductors, its vertical axis shows residual tensile stress after the shift perpendicular to the conductor axis. Each open circle indicates the averaged value of 5 points at each spacer's position. The residual tensile stress in the trial was about 5-40 MPa, which is lower than the calculated value of σ. It is supposed that the tensile stress by this method partly spread over each equator and it results in lower stress than the calculated value. Actually, tensile stress was observed over the equator in each measurement. Friction losses may also reduce the measured value. After all pushing process, it is expected that tensile stress rise by each section's piling up. The measured value of stress is a fraction of electromagnetic force applied to the conductors in operations. It is expected to restrict loosening coils in the process from construction to operation.

From these investigation, we conclude the method to be effective to improve the coil performance and thus we selected case(b) as the principal method for the real winding of the

LHD. We proposed a new coil winding method which enabled us to produce acquired tension along conductors. Through the real scale winding trial, this method was proved to be effective in increasing the accuracy of the helical coil. The application of this method can be expanded to the manufacture of other types of nonplanar coils in fusion devices to greatly increase the accuracy and reliability.

An additional on-site winding test was carried out before real winding of the LHD helical coil, and the effect of this method was verified.

C. *The Effects on Stability*

The achieved winding accuracy with this method is better than those of previous experimental coils by one order. This improvement is considered to be a major advantage to prevent the degradation of coils. To estimate the effects of this winding method on their stability, we can take two different criteria for evaluation. The following is a discussion concerning the stability of the LHD helical coils.

Assuming that the disturbance energy was integrated with time, i.e. the enthalpy of liquid helium around the conductor effectively removes heat and helps transition from the normal to the superconducting state, we can calculate a permissible energy which available helium can remove. Considering the latent heat of helium and its expansion by vaporization in limited cooling channels, the energy which the available helium can remove is about 0.4 J per one spacer. This allows about 0.4 mm of permissible wire movement, assuming an electromagnetic force on single conductor of 13 kA, 7T and a friction coefficient μ=0.3. We can see that only case (b) of Figure 4.2.6 satisfies this criterion. In practice, some points in the distribution of case (b) may be above this value, however the validity of this winding method was certified.

Assuming other kinds of disturbances – which are steeper, have shorter durations and are more probable in real magnets – we have to use the concept of MQE. As discussed in section 3-5, the permissible value of wire movement near recovery current is ranging from several μm to several tens of μm. Even the achieved value of winding accuracy on-site exceeds these values; above the recovery current, slightest movements of the conductors may cause quench in the magnets. We should classify their operation currents from the viewpoint of MQE and permissible wire movement. This will be summarized in section 5-3 considering the variation of recovery current discussed in section 3-5.

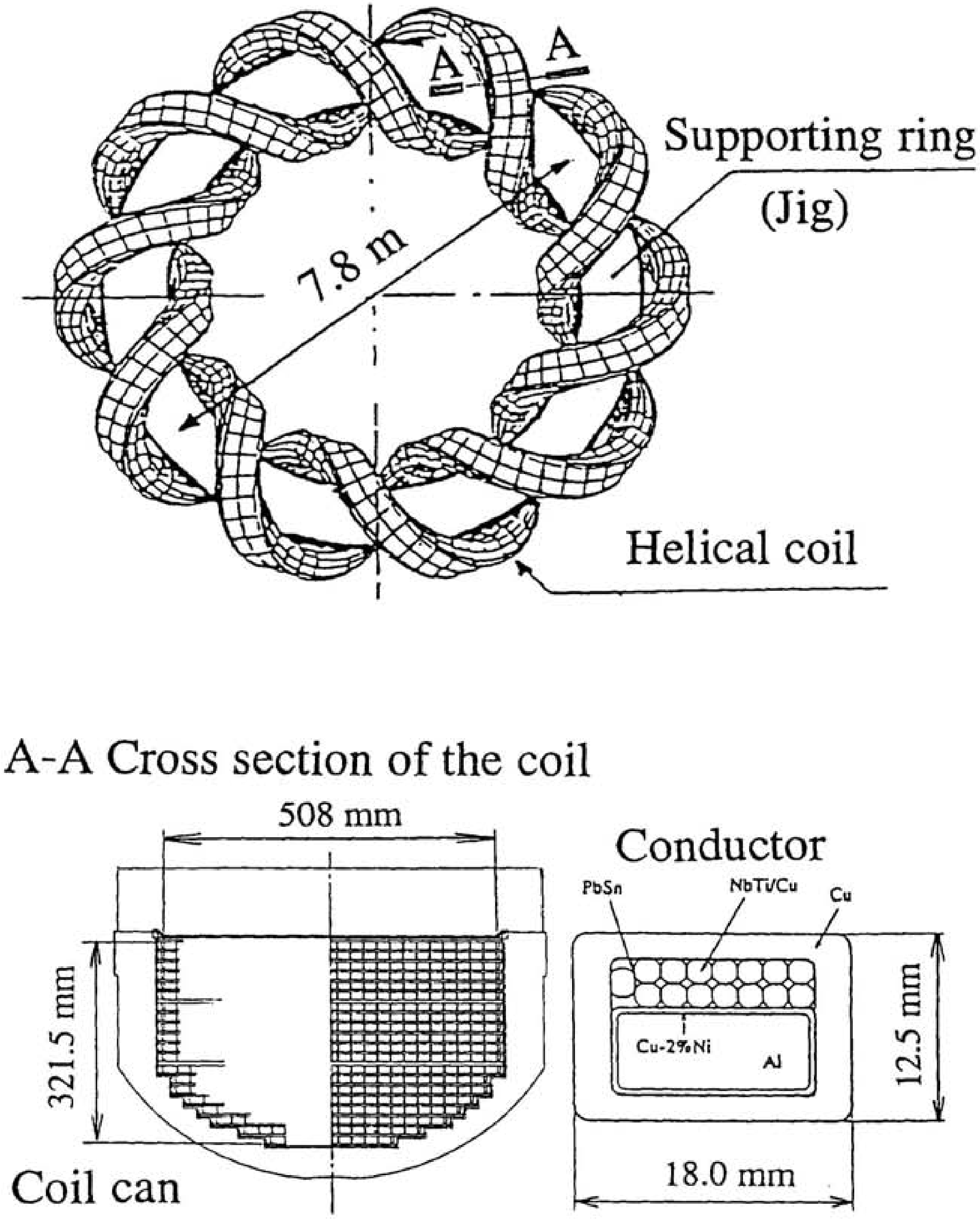

Figure 4.2.1 Overview and cross section of LHD helical coil and its conductor. The conductor has to be wound in accordance with its loci equation. Coil cans were assembled accurately on a torus-shaped supporting ring. They were used as bobbins during the winding process, and will be used as the helium bath after the completion of LHD. The supporting ring will be taken apart in pieces after the winding process.

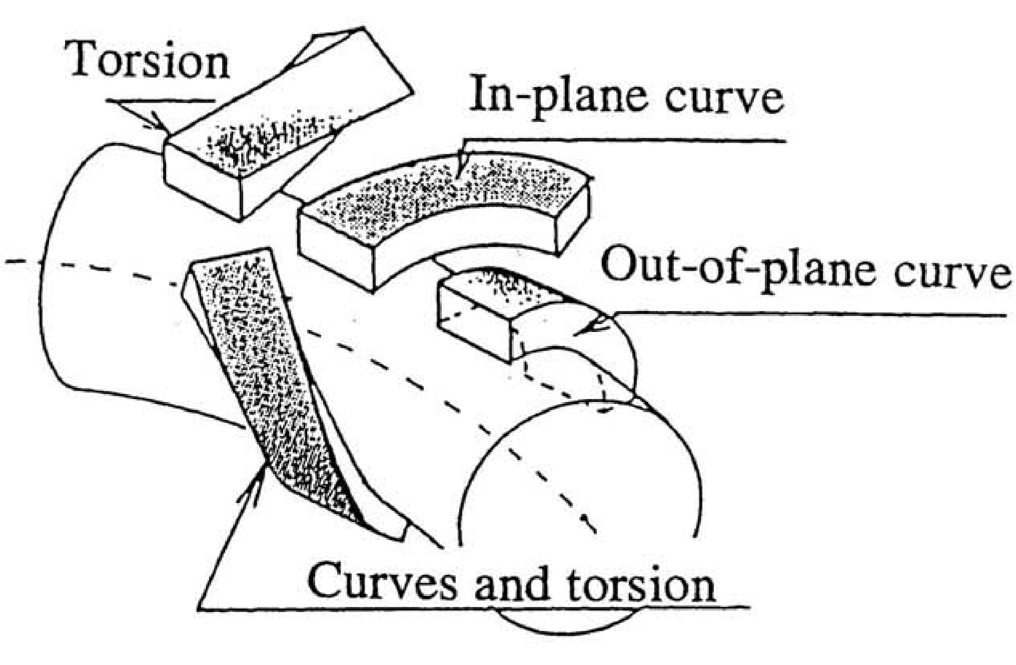

Figure 4.2.2 Curvatures and torsion of the helical coil. The locus of the helical coil has in-plane curvature, out-of-plane curvature, and torsion. Torus effect contorts the locus and produces in-plane curvature.

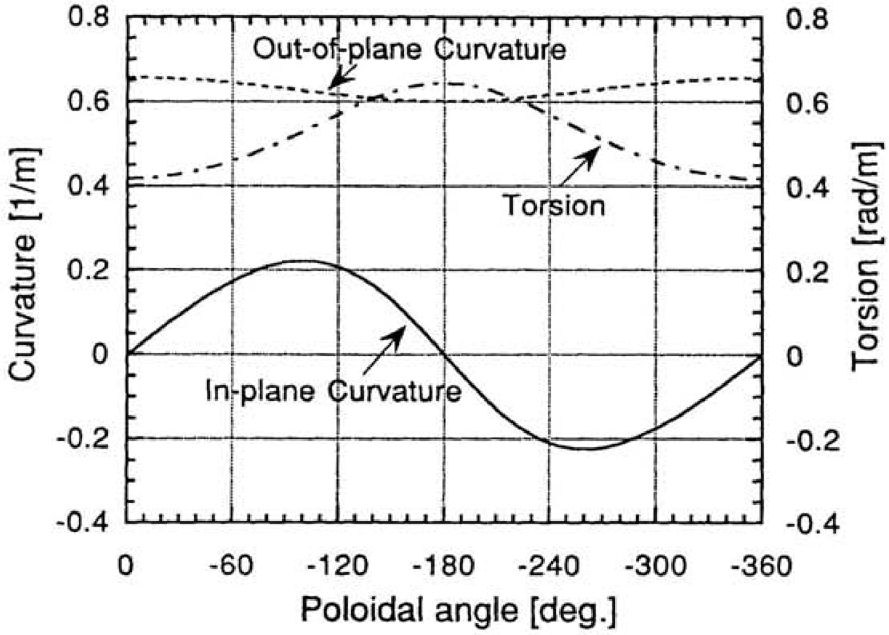

Figure 4.2.3 Typical profile of helical coil locus. These in-plane curvature, out-of-plane curvature, and torsion varies with the poloidal angle. The order of the out-of-plane curvature is several times larger than that of the in-plane curvature, but accurate forming of the in-plane curvature is crucial in helical coil winding.

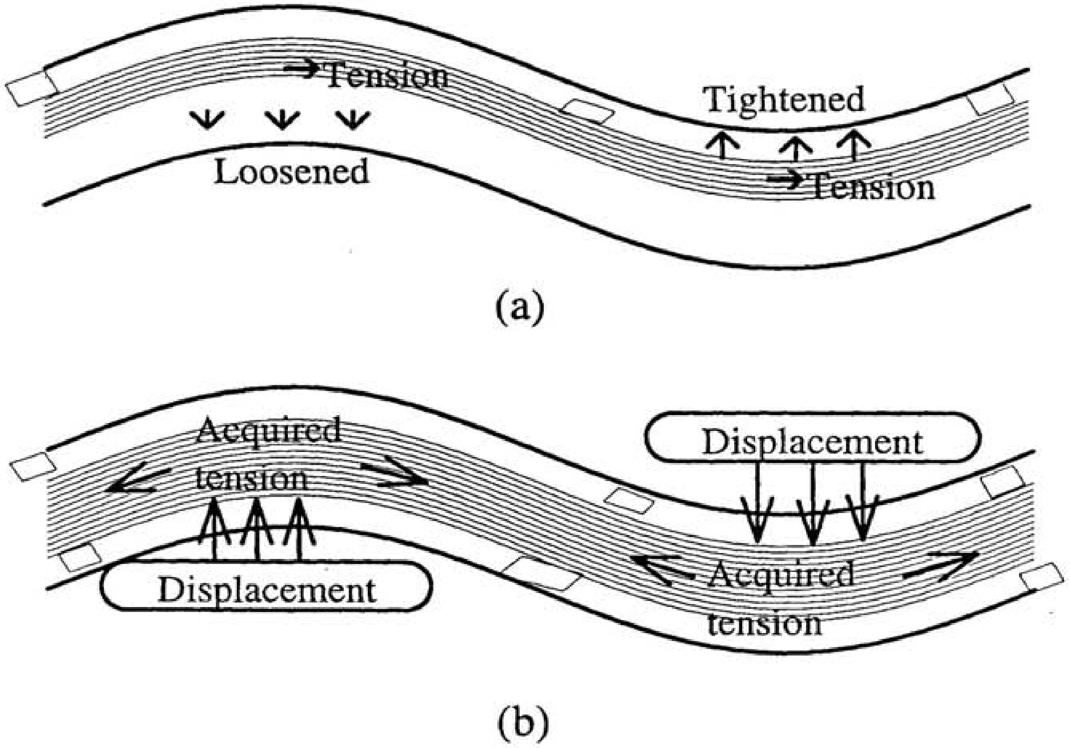

Figure 4.2.4 Concept of acquired tension winding method; development drawing along the helical coil. (a) External direct tension causes a shift of discrepancy perpendicular to the conductor axis and lessens the accuracy of the coil. (b) The acquired tension winding method. After each layer is wound, it is pushed to shift perpendicular to the conductor axis, from the shorter path's side to the longer path's side, utilizing its in-plane curvature. This displacement produces the acquired tension along the conductors and increases the accuracy of the coil.

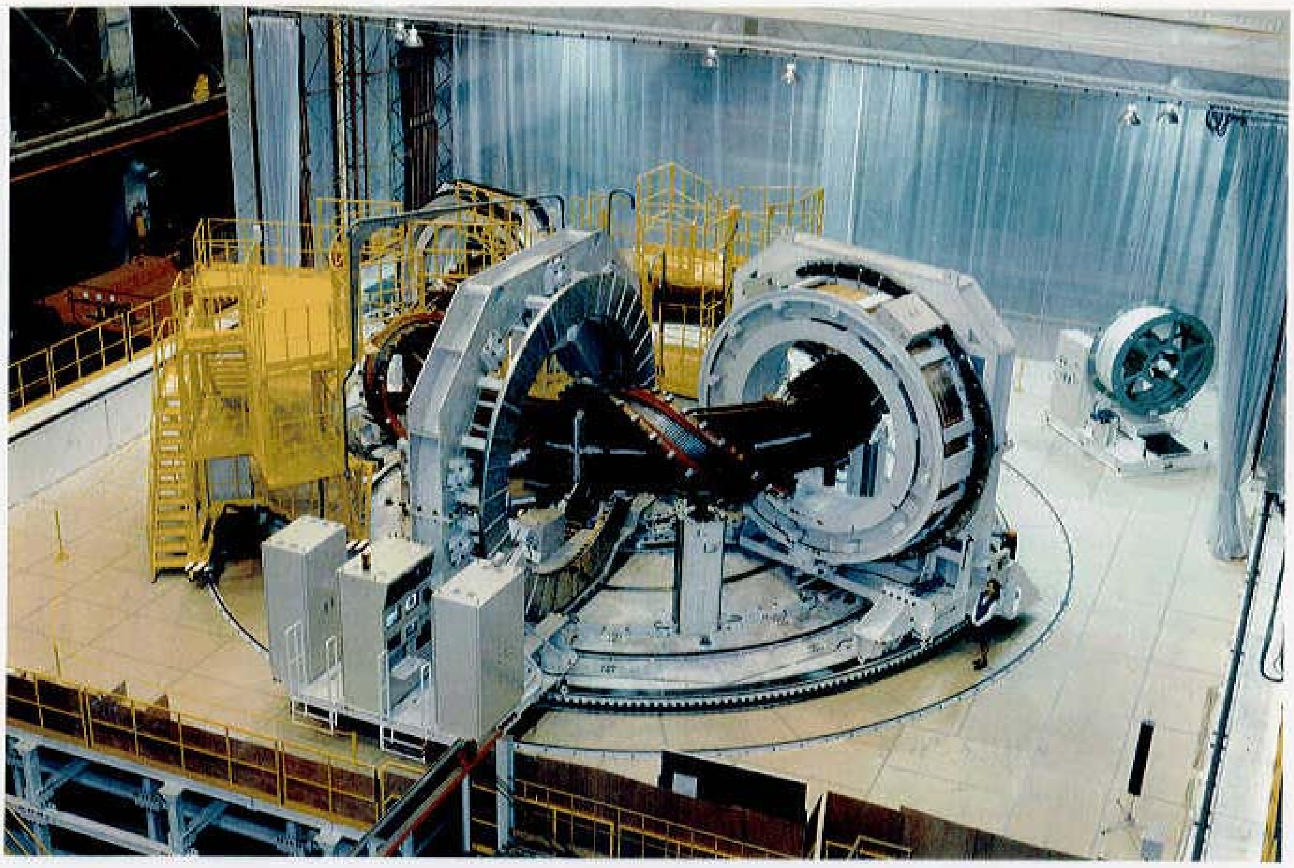

Figure 4.2.5 Winding machine and test coil for real-scale winding trial. The dimensions of the R&D test coil were to the real scale of LHD; its major radius was 3.9m, its minor radius was 0.975m. The test coil was a mock-up pool-cooled superconducting coil which was assembled from a coil can model, composite superconductors and insulation spacers. The conductor was formed into a helical shape by the forming head of the winding machine and fixed in the coil can. Many R&D items were carried out in this winding trial.

Table 4.2.1 Specifications of the Real-Scale Winding Trial

Item	LHD	the Winding Trial
Major radius (m)	3.9	←
Minor radius (m)	0.975	←
l	2	1
m	10	5
α (pitch modulation parameter)	0.1	0.1
Number of turns	450	> 22
Conductor	SC	←
Superconducting material	NbTi	←
Conductor dimension (mm)	12.5 x 18.0	←
Insulation spacer	GFRP	←
Spacer configrations	-	various types
Coil can	Stainless Steel	Fe + Stainless Steel
Winding machine	use	←
Winding method	plastic working + complementary methods	← + leveling + acquired tension, etc.
Winding location	on site	in works

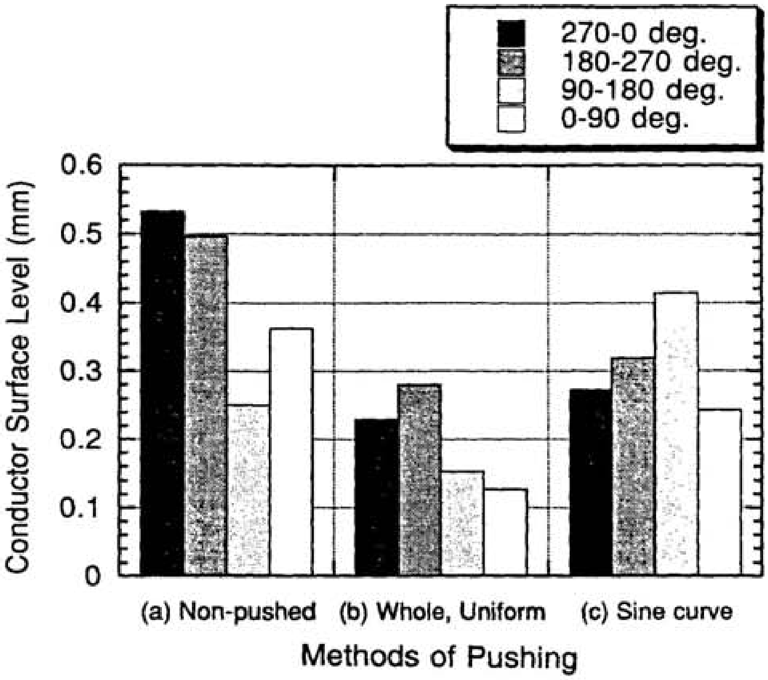

Figure 4.2.6 Variations of gaps between the conductor bottom surfaces and the insulator top surfaces. Case(a) indicates the non-shifted layer, case(b) indicates the layer which was pushed in the whole range with a uniform displacement and case(c) indicates the layer which was pushed with gradually changed values along the conductor following the sine curve. The results of cases(b) and (c) were better than that of case(a) in respect of reduced levels of the conductor surfaces . Case(b) was the best.

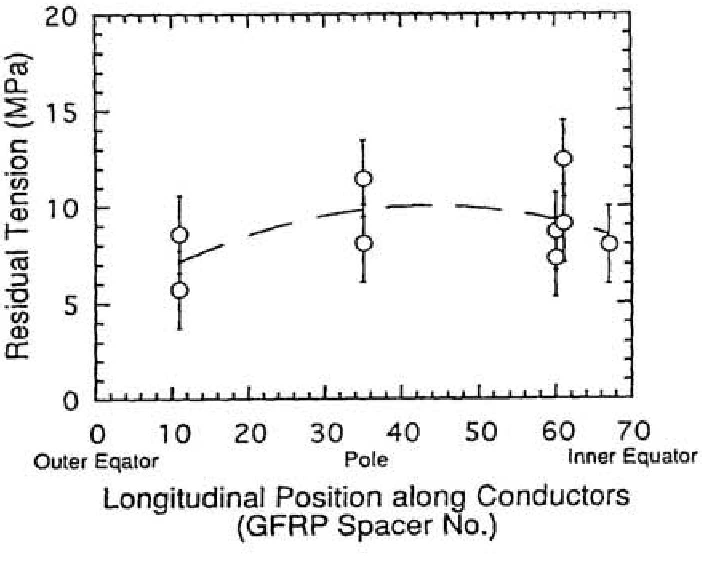

Figure 4.2.7 Residual tension versus longitudinal position along the conductors. Each open circle indicates the averaged stress value of 5 points at each spacer's position. Measured tensile stresses were lower than a typical calculated value, however, it is expected that this tensile stress will restrict the loosening of the coil during the process from its construction to its operation.

5. Conclusion

5-1. The Thermal Behavior of Composite Superconductors

The accurate MQE value can be obtained by employing both experimental measurement with heaters and analytical estimation of heating efficiency. The experimental MQE values can be gathered by simulating disturbances in short sample superconductors at set transport currents and background magnetic fields. The disturbances are caused mainly by the friction the electromagnetic force creates between conductors and insulations. The measured MQE values, however, usually contain errors caused mainly by the longer response times of heating devices compared with the thermal diffusion time constants of conductor materials. These errors can be eliminated by two-dimensional thermal analysis. This computed MQE value was smaller than the measured MQE value by one order, and it conformed with the enthalpy of the heated region of the conductor.

The stability margin of a conductor varies with the direction of the heat flux when the conductor is marked by thermal anisotropy, which in the one used in LHD helical coils derives from its geometry. In real magnets, the direction of heat flux cannot be expected to be uniform because the distribution of electromagnetic force is not uniform. The computed MQE value was smaller because the conductor's thermal anisotropy had been taken into account, and it must be applied in magnet operation.

The accurate MQE value can still be obtained by employing an experimental formula when the disturbances in a magnet are distributed. The MQE value per heated spot at distributed disturbances approaches half of the value at point disturbance, and total energy increases with the number of heated spots.

The relation between conductor displacement and released energy can be determined with the electromagnetic force in the coil and the friction coefficient between its conductors and insulators. Equating the computed MQE with the released energy reveals the permissible displacement of a conductor, i.e. the permissible gap between the conductors and the insulators. It is one of the benchmarks in determining coil structure and winding accuracy.

The MQE measurements differ from each other according to sample and sample part. Even in the same experimental setting, the differences can be considerable. Some differences are inherent in conductor performance, while others are simply experimental errors; however, they cannot be distinguished. The smaller MQE values should therefore be applied in safe magnet operation.

5-2. The Advanced Winding of Superconducting Helical Coils

We aimed at preventing degradation of the coils, in particular, at reducing as much as possible the magnitude and probability of mechanical disturbances in the coils. The following steps improved the accuracy of winding coils and formed part of the research and development concerning LHD.

1. An experimental helical coil with cooling channels, TOKI-WT, was constructed. It demonstrated the necessity continuously to adjust the shape of the conductors.

2. An experimental superconducting helical coil, TOKI-HB, was constructed. It demonstrated the effectiveness of the winding machine for continuous conductor forming, but also the necessity deliberately to create tension in the coil with a complementary winding method.

3. A real-scale winding trial was carried out. It demonstrated the effectiveness of the newly developed method, which utilizes the three-dimensional shape of helical coils and makes it possible to create tension after the usual winding process, leading to superior coil winding accuracy.

Our method can be applied to the manufacturing process of any helical coil, but it is particularly valuable for superconducting helical coils which have cooling channels.

5-3. The Stability of the Large Helical Device (LHD)

In the LHD helical coils, degradation might well be smaller than in the experimental coil, which simulated LHD operation currents and background magnetic fields. Winding accuracy in the actual winding process is much improved. The proportion of wet to total conductor surface will be larger than in the short samples, so cooling should also be improved. These advances will increase the stability of the LHD and make it possible to reach the operation current (I_{op}) while keeping it below the recovery current (I_r).

The following predictions of LHD operation can be deduced from the results of short sample conductor tests and a previous experimental coil. The above-mentioned advances were not taken into consideration, and the degradation rate of 20 % was based on recovery current measurements in the experimental coil of section 3-5.

(a) $I_{op} \leq 11$ kA (80 % of experimental conductor $I_r = 13.7$ kA)

In this region, the operation current is below the recovery current even when allowing for 20 % of degradation. The coil will not quench and the magnet can be operated without serious difficulty. At an operation current of 11 kA, the central magnetic field will be 2.5 T, which is larger than 2.0 T, the saturation field of iron. At this point, the operation will already be taking advantage of the conditions in superconducting magnets.

The data acquired in this region will be of great help in predicting LHD performance at higher currents, so various diagnostic techniques and analyses (e.g. voltage spike observation, strain and acoustic emission measurement) will be employed.

(b) 11 kA $< I_{op} <$ 13 kA (rated current of phase I)

In this region, wire movement, caused by electromagnetic force, will probably be greater than the permissible wire movement, derived from MQE values for transport currents near the recovery current and ranging from several μm to several tens of μm. It will be necessary to energize the coils slowly and carefully, and to apply the experience gained in the preceding region (a) as well as findings gathered while monitoring the operation.

(c) $I_{op} = 13$ kA

When the operation current finally equals the rated current of phase I, the permissible disturbance energy will be quite small, ranging from several mJ to several tens of mJ. Any kind of disturbance must be kept to the minimum, particularly controllable factors like excess ac losses caused by poloidal field variation.

Figure 5.3.1 shows areas of stability of the LHD helical coils. Magnet stability is determined by several factors. Which of them is the main factor depends on the operation region and the behavior of the liquid or gaseous helium:

(A) Below the recovery current, magnet stability is determined mainly by the enthalpy of the liquid helium in the limited space of the cooling channels. The above-mentioned operation regions (a), (b), (c) are included in this area, but it should be noted that the recovery currents of the magnet and the conductor might be different because of degradation, a larger exposure rate, and other reasons. The LHD helical coils have to be operated in this area.

(B) Above the recovery current, magnet stability is determined mainly by the enthalpy of the conductor, and MQE values are therefore much lower here than in area (A).

(C) Below the recovery current, in the special case that an extremely large amount of gaseous helium blocks the cooling of the conductor, magnet stability is determined mainly by the enthalpy of the conductor.

We hope that our work is a valuable contribution to the design, construction and operation of superconducting magnets. Learning about the behavior of liquid and gaseous helium in finite cooling channels will be an important next step.

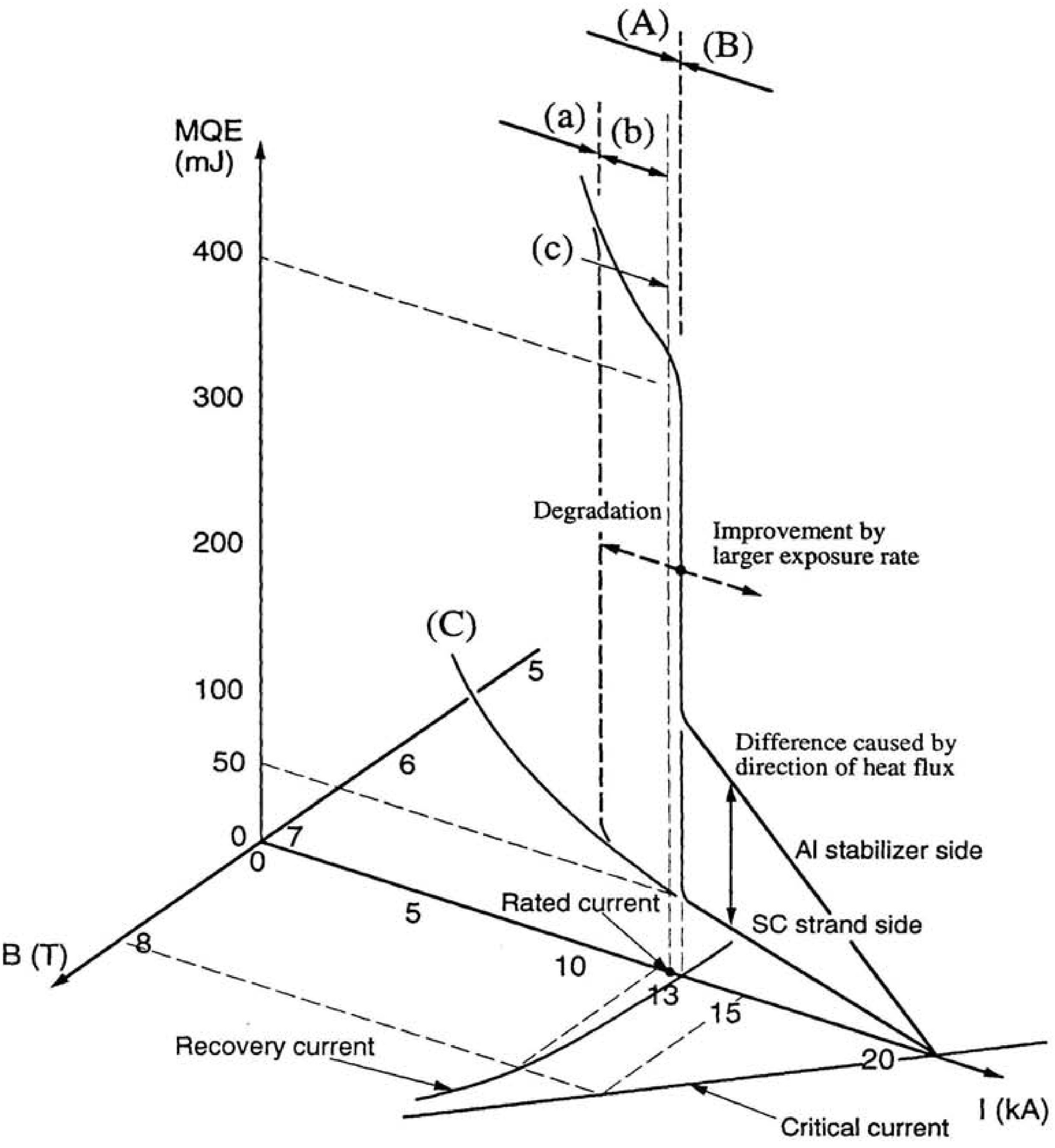

Figure 5.3.1 Stability of the LHD helical coils [at 7 T - peak magnetic field of the magnet]. Which is the main factor of magnet stability depends on the operation region and the behavior of the liquid or gaseous helium: (A) Below recovery current. (B) Above recovery current. (C) Below recovery current, in a special case (see text).

References

[1] Lyon, J. F., "Near-Term Directions in the World Stellarator Program", Fusion Technology 17 (1990) 19.

[2] Iiyoshi, A. et al., "Design Study for the Large Helical Device", Fusion Technology 17 (1990) 169.

[3] Motojima, O. et al., "Physics and Engineering Design Studies on the Large Helical Device", Fusion Engineering and Design 20 (1993) 3.

[4] Yamazaki, K. et al., "Requirements for Accuracy of Superconducting Coils in the Large Helical Device", Fusion Engineering and Design 20 (1993) 79.

[5] Harris, J. H. et al., "Realization of the Advanced Toroidal Facility Torsatron Magnetic Field", Fusion Technol. 17 (1990) 51.

[6] Mathis, R. and Sapper, J., "Design and Engineering Aspects of the Main Components for the Wendelstein VII-AS Stellarator Experiment", Fusion Engineering and Design 11 (1990) 399.

[7] Ito, S. et al., "High-field Tokamak TRIAM-1 M with Superconducting Toroidal Magnets", Proc. 11th Eur. Conf. (Aachen, 1983) A 04.

[8] Truck, B., "Six Tears of Operating Experience with Tore Supra, the Largest Tokamak with Superconducting coils", Presented at MT-14 (Tampere, 1995) B14

[9] Haubenreich, P.N. et al., "Superconducting Magnets for Fusion", Nucl. Fusion 22 (1982) 1209.

[10] Iiyoshi, A. and Yamazaki, K., "The Next Large Helical Devices", Phys. Plasmas 2 (1995) 2349.

[11] Beilder, C. et al., "Physics and Engineering Design for Wendelstein VII-X" Fusion Technology 17 (1990) 148.

[12] Yamamoto, J. et al., "Research and Development of Superconductors an Superconducting Coils for the Large Helical Device", Fusion Engineering and Design 20 (1993) 139.

[13] Motojima, O. and LHD Design group, "Design Status of Superconducting Large Helical Device", IEEE Trans. on Magnetics 27 (1992) 2214.

[14] Sakamoto, M. et al., "Excitation Experiments of Module Coil (TOKI-MC) as an R&D Program for Large Helical Device", IEEE Trans. on Appl. Superconductivity 3 (1993) 543.

[15] Mito, T. et al., "Stability Tests of Module Coil (TOKI-MC) Wound with an Aluminium Stabilized Superconductor", IEEE Trans. Mag. 27 (1991) 2224.

[16] Mito, T. et al., "Effects of Spatially Limited External Magnetic Fields on Short Sample Tests of Large-Scale Superconductors", Presented at MT-14 (Tampere, 1995) B71.

[17] Wilson, M.N., "Superconducting Magnets", Clarendon Press, Oxford (1983).

[18] Stekly, Z.J.J. and Zar, J.L.,"Stable Superconducting Coils", IEEE Trans. Nucl. Science 12 (1965) 367.

[19] Maddock, B.J. et al., "Superconducting Composites : Heat Transfer and Steady State Stabilization", Cryogenics 9 (1969) 261.

[20] Martinelli, A.P. and Wipf, S.L., "Investigation of Cryogenic Stability and Reliability of Operation of Nb3Sn Coils in Helium Gas Environment" Proc. Appl. Superconduc. Conf. (IEEE Pub. 72CHO682-5-TABSC, 1977) 3311.

[21] Senba, T. et al., "A Real-Scale Helical Coil Winding Trial of the Large Helical Device" Fusion Technology 1994 vol.2 (1995) 905.

[22] Nishimura, K. et al. "Compact Helical System Physics and Engineering Design" Fusion Technology 17 (1990) 86.

[23] Imagawa, S. et al., "Construction of Helical Coil Winding Machine for LHD and On-site Winding" Presented at MT-14 (Tampere, 1995) B10.

[24] Imagawa, S. et al., "Optimization of Wetted Surface Fraction of Helical Coil for LHD" Cryogenics 1994 Vol. 34 ICEC Supplement (1994) 701.

[25] Mito, T. et al., "Short Sample Tests of Aluminum-Stabilized Superconductors for Large Helical Device" Fusion Engineering and Design 20,(1993) 233.

[26] Yanagi, N. et al., "Experimental Observation of Anomalous Magnetoresistivity in 10-20 kA class Aluminum-Stabilized Superconductors for the Large Helical Device" Adv. Cryogenic Engineering Materials 40 (1994) 459.

[27] Yanagi, N. et al., "Aluminum Stabilized Superconductor for the Helical Coils of Large Helical Device - Development, Manufacturing, Testing and Joints -" Proc. 9th US-Japan workshop 'High-Field Superconducting Materials, Wires and Conductors' (Kyoto, 1995) 5.

[28] Kaneko, H. and Yanagi, N., "Enhancement of the Magnetoresistance due to Hall Current in Alminium - Copper Composite" Cryogenics 32 (1992) 1114.

[29] Imagawa, S. et al., "Analysis of Anomalous Resistivity in an Aluminium Stabilized Superconductor for the Large Helical Device" Adv. Cryogenic Engineering Materials (1994) 469.

[30] Iwasa, Y., "Case Studies in Superconducting Magnets" Plenum Press, New York (1994)

[31] Seo, K. et al., "Minimum Quench Energy Measurement for Superconducting Wires" Presented at MT-14 (Tampere, 1995) G26.

[32] Steward, W.G., "Transient Helium Heat Transfer: Phase I - Static Coolant" Int. J. Heat Mass Transfer 21 (1978) 863.

[33] Nara, K., "Thermometry at Cryogenic Temperatures" Cryogenic Engineering 27 (1992) 114 (in Japanese).

[34] Imagawa, S. et al., "Manufacturing of Compact Helical System" Fusion Technology 1998 (1989) 412.

[35] Sapper, J and W 7-X Technical Group, "Superconducting coil development for the Wendelstein 7-X stellarator" Fusion Engineering and Design 20 (1993) 23.

[36] Alejaldre, C., et al., "TJ-II Project: A Flexible Heliac Stellarator" Fusion Technology 17 (1990) 131.

[37] Yanagi, N. et al., "Design and Fabrication of Pool Cooled Helical Coil as an R&D Program for Large Helical Device" IEEE Trans. on Magnetics 27 (1991) 2357.

[38] Senba, T. et al., "Design and Construction of the Helical R&D Coil (TOKI-HB)" Fusion Engineering and Design 20 (1993) 195.

[39] Yanagi, N. et al., "Cooldown and Excitation Experiment of SC Helical Coil (TOKI-HB) as an R&D Program for Large Helical Device" J. Soc. Plasma Sci. Nucl. Fusion. Research. annual. conf. (1992) 29aB4.

[40] Tuda, Y. et al., "First Construction of a Superconducting Helical Coil for Feasibility Study of Large Helical Coil" Proc. MT-11 (Tsukuba, 1989) 789.

[41] Kitamura, K. et al., "Mechanical Analysis and Fabrication of the R&D Forced-Flow Helical Coil (TOKI-TF)" Fusion Engineering and Design 20 (1993) 167.

[42] Senba, T. et al., "An Advanced Method for Helical Coil Windings in Fusion Devices" Trans. Fusion Technology 28 (1995) 571.

[43] Iwamoto, A. et al., "Dependence of Heat Transfer from a Wide Copper Plate to Liquid Helium on Heat Transfer Surface Orientation and Treatment" presented at Int. Symposium. on Safety of Superconductors and Related Heat Transfer at Low Temperatures (Fukuoka, 1994).

[44] Iwasa, Y. et al., "Frictional Properties of Metal-Insulator Interfaces" IEEE Trans. on Mag. MAG-15 No.1 (1979) 36.